Barcelona Supercomputing Center
Centro Nacional de Supercomputación

Barcelona, 15 December 2015

Dear Editor,

Please find the revised version of our manuscript ***gmd-2015-162*** entitled "FPLUME-1.0: An integral volcanic plume model accounting for ash aggregation". We have improved the formulation of the energy conservation expressing it in terms of enthalpy and addressed all the points raised by the reviewers and our answers are detailed in the author's response. Please do not hesitate to contact us for any further clarification.

Best regards,

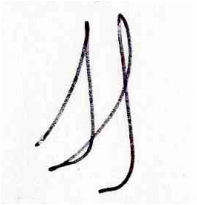

Dr. Arnau Folch Duran

Barcelona Supercomputing Center – Centro Nacional de Supercomputación
Edificio Nexus II. C/ Jordi Girona, 29. 08034 Barcelona
Tel. 934137716. Fax: 934137721.

Referee#1 (T. Espositi Ongaro)

Referee#1 General Comments

- *I only have one remark on the title, where "integrated" seems to indicate the integration (collection), in the same tool, of different features.*

  Title has been changed
- *The numerical algorithm is not much detailed (see Specific Comment below), nor a manual is provided as a supplement, but a thoroughly commented source code can be obtained upon request.*

  It has been stated that code is available under request and the manual will be provided with the distribution package.

Referee#1 Specific Comments

Section 2.1

- *Equation 2c) lacks a term associated to the mass loss. If it is neglected, the reason should be specified.*

  The term is implicitly included in P (LHS).
- *Line 20, p.8016) I see no reason to use such an approximate equation of state (even though the approximation is probably good "almost" everywhere).*

  Right. The sentence has been removed
- *Equation 15) I would like to know whether this equation is inverted (and how) to compute the settling velocity (Eq. 14): the Reynolds number (Re) is indeed a function of the non-equilibrium velocity, and this makes the inversion not immediate.*

  We have added the sentence "Given that the Cd depends on Re (i.e. on us), Eq. 14 is solved iteratively using a bisection algorithm."

Section 2.2

- *Equation 19) Please explain why the sin(theta) factor in the second term in the RHS "generalizes" Eq. 18.*

  We have added the sentence "Beside the local Richardson number, the entrainment coefficient αs depends on plume orientation (e.g. Lee and Cheung, 1990; Bemporad, 1994), therefore we modify Eq. 18 as:" and 2 new references.
- *Equation 20) The choice of the interpolation function is not justified enough. Looking at Figure 2, the interpolation function seems quite arbitrary, given that it extends over two orders of magnitudes of zs. It is also different, for high zs, to the*

interpolation function proposed by Carazzo et al. (2008). I understand the need of having an analytical expression in the whole range, but it would be useful to know how this choice impacts the results. Equation 21) This is an unpublished results from a PhD thesis. As for the previous point, I do not see here a major improvement with respect to a model with constant entrainment parameterization.

In order to answer to this point (and also to the main comment from reviewer#2) we added a sentence at the end of section 2.2 where we stress the limitations of the entrainment parameterizations. Concerning the interpolation function, it is clearly stated that is an empirical function. Finally, eq (21) comes from a published work (the PhD Thesis is available online).

- *Figure 3) If possible, plot the entrainment coefficients against the non dimensional scale Zs.*

  Done. Figure 3 has been changed

Section 2.3

- *Eq. 23) holds for a vertical plume with constant entrainment, so it seems difficult to justify it for bent-over plumes with variable entrainment. Therefore, I am wondering whether it would not be better to compute Ht simply by means of the Bernoulli equation along a plume streamline and for an adiabatic transformation.*

  We agree with the referee. We have added the sentence "In the umbrella region (from the NBL to the top of the column), we neglect air entrainment and assume that the mixture is homogeneous, i.e. the content of air, water vapor, liquid water, ice, and total mass of particles do not vary with z." Regarding the Bernoulli equation, we disagree with the reviewer, as the umbrella region is an open system (calculation by the reviewer were probably made assuming a homogeneous environment with constant density and pressure).

Section 3

- *The assumption that all particles aggregate into a single particle class seems rather simplistic, although it is clear from the paper that more complex models would probably be poorly constrained by data. Although I understand that such an assumption strongly simplifies the computation, I would encourage the authors to discuss how the aggregation model would be modified if this hypothesis was relaxed and a spectrum of aggregates had to be considered.*

  We have added the sentence "Obviously the assumption that all particles aggregate into a single particle class is simplistic and considering a range of aggregating

classes would be more realistic. However, there are no quantitative data available for such a calibration."

- *Lines 7-17 p.8030) These considerations should be supported by evidences or references to previous works.*

  We have added the references (Costa et al., 2010; Folch et al., 2010)

- *Last paragraph, p.8030-8031) I suggest to move this paragraph in Section 4 (model algorithm). In addition, the algorithm should be described in more detail: since A+ and A- (computed at step 8) affect the solution of the system of transport equations (solved at step 1), I would like to understand how is this dependency solved numerically (is it a predictor-corrector algorithm?).*

  Following referee's suggestion, we have moved the paragraph to the end of section 4. It is now clear that the package lsode is used for solving the system of equations.

Section 5

- *Lines 25/27, p.8033) Are the two values of Dfo inverted?*

  Yes, this has been corrected

- *Lines 16-18, p.8035) "Input values… vent coordinates". Move this sentence at line 29 after "…height".*

  ok

- *Line 28, p.8035) To understand how Fig. 10 was constructed, the ranges of variability of the input parameters in the study should be specified.*

  We have added the sentence "Input parameters were fixed as in Table 5 varying only column height from 4 to 8.5 km (a.v.l.)" at the caption of Figure 10.

- *Fig. 10) This figure is interesting but might be misleading, since it seems to suggest a direct dependency or control of the mass fraction of aggregates of the column height, which would be surprising. The discussion of this figure (page 8036) should be extended, by commenting the main source of variability of the column height. If possible, also substitute the continuous line with symbols.*

  We have added the sentence "However, it should be kept in mind that mass fraction of aggregates is not controlled by the eruptive column height but depends on several variables such as particle concentration (that is a function of the mass flow rate), presence of liquid water (that can form above a given level depending on the local meteorological conditions), etc." at the end of section 5. An axis showing the corresponding MER has been added to Figure 10.

Other corrections

Finally, we have accepted the minor corrections on the annotated manuscript.

Referee#2 (anonymous)

Referee#2 General Comments

- *I would like them to provide more justification of the form of their entrainment coefficient. This seems to be based on the similarity drift observed by Kaminski et al. (2005) (and later by Carazzo et al. 2006, 2008). However, the veracity of this similarity drift is inconclusive: it was not observed by Wang and Law (JFM, 2002) in their experiments nor has it been seen in DNS or LES of buoyant plumes (see papers by van Reeuwijk and co-workers especially JFM 2015). It may simply be an artefact of Kaminski et al.'s experiments and for this reason I am somewhat sceptical of its adoption in volcanic plume models.*

We agree with the referee. We have highlighted that FPLUME can consider different options, in particular user-defined constant coefficients or the parameterization based on the local Richardson number. We have also add the sentence "However, the veracity of the empirical parameterization in Eq. (18) was not observed by Wang and Wing-Keung Lawin (2002) in their experiments nor has it been seen in DNS or LES simulations of buoyant plumes (Craske et al., 2015)". In addition, we have also added a paragraph at the end of section 2.2.

Referee#2 detailed Comments

- *p. 8010, l. 26. Buoyancy drives the plume upwards below the NBL; above the NBL the buoyancy is negative. I would delete the sentence from `above' onwards; you also need to insert `to' after `leads'.*

  ok
- *p. 8011, l. 2 Momentum reaches a maximum at the NBL and carries the plume upwards above the NBL for all plumes regardless of eruption strength.*

  The sentence now reads "Excess of momentum above the NBL (overshooting) can drive the mixture higher forming the umbrella region, where tephra disperses horizontally first as a…"
- *p. 8011, l. 5+ I didn't understand the sentence beginning `Depending on the balance...'*

  Sentence has been removed.

- *p. 8011, l. 10 I didn't understand what is meant by `characterization trough observations'*

  The sentence now reads “Quantitative observations and models of volcanic plumes are…”
- *p. 8011, l. 14 `build' ! `built'*

  ok
- *p. 8011, l. 18 `its' ! `their'*

  ok
- *p. 8011, l. 28 Woods (1988) does not include moisture.*

  Right, reference removed.
- *p. 8012, l. 14+ Can the authors substantiate their claim that atmospheric dispersion models without aggregation over predict ash concentrations in the far field? While this seems plausible, aggregation may reduce fall speeds by increasing the drag (more irregular shapes) and reducing the effective density (relative to a single particle of the same size). I think one needs to be careful with what is being compared with what, and what is being kept fixed as the reference point. I would make the statement less strong.*

  Yes, aggregation reduces effective density and hence fall speeds (relative to a single particle of the same size). However, this effect is highly counterbalanced by the velocity increase due to the size of aggregates compared to the primary particles given the d^2 dependency.
- *p. 8012, l. 24 `bent' ! `bending'*

  ok
- *p. 8013, l. 10 `specie' ! `species'*

  ok
- *p. 8013, l. 23 I didn't understand `univocally'.*

  Word removed
- *p. 8016, l. 6 `in' ! `on'*

  ok
- *p. 8023, l. 4 `than' ! `as'*

  ok

- *p. 8023, l. 8+ Do the authors have any evidence that there is no entrainment in the umbrella region? The dynamics of the region are clearly complicated but the flow is turbulent which suggests entrainment has at least the potential to take place.*
  We have added the reference Costa et al. (2015) as support. See also the changes in section 2.3 with respect to the original version.
- *p. 8025, Eq. (28) I'm assuming that the sum over all Aj has index k? Is this correct?*
  Yes, equation corrected
- *p. 8025, l. 16 `where' ! `were'*
  ok
- *p. 8027, l. 1 `to' ! `in'*
  ok
- *p. 8027, l. 11 Insert `a' after `as'*
  ok
- *p. 8028, l. 6 Insert `to' after `respect'*
  ok
- *p. 8030, l. 8 `meet' ! `met'*
  ok
- *pp 8032-8034 Regarding Fig.7, could the authors comment on why the model and observations agree better for small and large values of but not intermediate values?*
  These are not "observations" but comparison with a parameterization (Cornell) based on observations. Comparison makes sense only for ϕ larger that that of aggregates.
- *p. 8034, l. 3 `allows to' is not grammatically correct. Something like `... is that it allows estimation of the fraction ...'*
  ok
- *p. 8034, l.17 Remove `a'*
  ok
- *p. 8034, l. 18 `on' ! `in'*
  ok
- *p. 8034, l. 19 `along' ! `during'*
  ok

Referee#3 (anonymous)

Referee#3 detailed Comments

- *Title: maybe the present title can be misunderstood; it could explicitly states that the model is accounting for other important phenomena rather than only ash aggregation. I admit it might be quite long then...*

  We modified already the title as suggested by reviewer #1 but we prefer to keep the emphasis on ash aggregation as, although the code is very general and account for several processes, it is the new feature among 1D plume models.
- *Abstract: as the 1.0 version of the model is presented here, it would be nice to end by a sentence announcing future/potential improvements.*

  We added the sentence: "The modular structure of the code facilitates the implementation in the future code versions of more quantitative ash aggregation parameterization as further observations and experiments data will be available for better constraining ash aggregation processes."
- *p8010-l19: maybe state that volcanic plume are turbulent flows*

  OK
- *p8010-l23: "negatively buoyant basal thrust region"*

  OK
- *p8011-l09: you may wish to add a couple of references here, e.g. Carazzo et al. 2014 (Laboratory experiments of forced plumes in a density, stratified crossflow and implications for volcanic plumes, Geophysical Research Letters 41 (24), 8759-8766)*

  OK
- *p8011-l17: I would add that sophisticated 3D multiphase models have problems on their own related to the accurate description of the physical processes their are taking into account (e.g., closure equations, impact of spatial resolution, etc).*

  OK, a sentence added
- *p8012-l5: the upcoming special issue of the Journal of volcanological and geothermal research might be cited (if time has come).*

  Done
- *p8013-l2: for sure the TGSD is also depleted in large particles related to the source due to sedimentation.*

This fact is not relevant for ash aggregation that involves fine ash only.

- *p8014-l5: I suggest to define the mass, momentum, energy fluxes as well as s before giving the equations of conservation that will give their evolution with z. The parameters related to aggregation in the equations should be defined in the main text here (rather than in page 8016) as they are key in the paper (I mean not only in the table at that stage), as well as the rate of entrainment.*

  OK, done

- *p8015-l25: this is a detail, but one may note that buoyancy main become positive in the basal gas-thrust region (i.e. before the source momentum has become negligible).*

  We added "generally" in the revised version

- *p8016-l18: is rho_p independent of the size of the particles?*

  Yes, is the weighted average of all particle classes. We clarified this point.

- *p8019-equ(5): is this formula equivalent e.g. to the ones used in Girault et al. 2014 (The effect of total grain-size distribution on the dynamics of turbulent volcanic plumes, Earth and Planetary Science Letters 394, 124-134)? If not, what are the implications of the choice made here?*

  On pag 8019 there is no eq. (5) but eq. (15) that refers to a well-known experimental parameterization describing settling velocity of non-spherical particles. Eq. 5 is the definition of the partial pressure of water vapour.

- *p8021&8022: variable entrainment. I have two questions on that part: - for sure a volcanic plume is a forced jet in the basal gas-thrust region. Hence I do not see why it is necessary to propose a function for A_plume(zs) for zs<10. I wonder also why A_jet(zs<10) cannot be taken as A_jet(zs=10) rather than proposing an unconstrained function. Does that choice really affect the results? I guess it does not, but if it is the case this as to be discussed as the model would then appear open-ended.*

  This choice was made to have a general formulation with reasonable limit conditions that can be extended even outside of the values characterizing volcanic plumes. However in the new version of the plots we used as well zs as variable so it is easier to see typical ranges of volcanic plumes.

- *I am not sure I understand why a sin(theta) is added in equation (19). Could you add a few sentences to explain that point in more details?*

We added the original references were this correction was firstly proposed.

- *p8023-equ(23): isn't there more recent ways to determine H_t? I think there is at least one paper by Koyaguchi and Suzuki that compare the evolution of Ht and Hb with the eruptive flow rate. This part of the model appears less convincing than the previous one adressing the dynamics of the plume below the NBL. Is there a way to show that the approach (i.e., the prediction of the total height Ht) is consistent with some results from 3D numerical models or lab-scale experiments?*

  OK. We added the following sentence at the end of the section: "Although the proposed empirical parameterization of the region above the NBL is qualitatively consistent with the trends predicted by 3D numerical models (Costa et al., 2015), a more rigorous description requires further research."

- *p8024-l10: Plume wet aggregation model. This part is the most difficult to read as many equations are presented that involved a large number of parameters. I wonder if it is possible to have an idea on the dependence of the model results on these various parameters. I understand that Df0 is the key parameter here, but it will be good to illustrate more its importance relative to other parameters. It will be good also to show a figure with the evolutions of the predictions of the model when starting from a model with no aggregation and then adding the different processes ending to the full variation of n_tot (equ 34).*

  Yes, unfortunately the physics of particle aggregation are controlled by several variables in a nonlinear way and a simple study as the one the reviewer suggested will be very partial anyway. The model we used is described and discussed in Costa et al. (2010) and Folch et al (2010).

- *p8034-l15: Eyjafjoll eruption: did you consider the possible presence of meteoritic water in the plume, and will this affect the results (aggregation made easier)?*

  This is a good point and the meteoric water can enhance aggregation. Unfortunately we have not considered this effect, as reliable data are not available for the day of the eruption. In the revised version we clearly stated this point adding: "moreover the presence of meteoritic water in the plume (not considered here) could significantly enhance aggregation."

Manuscript prepared for Geosci. Model Dev.
with version 2014/09/16 7.15 Copernicus papers of the LaTeX class copernicus.cls.
Date: 18 December 2015

FPLUME-1.0: An ~~integrated~~ integral volcanic plume model accounting for ash aggregation

Arnau Folch[1], Antonio Costa[2], and Giovanni Macedonio[3]

[1]CASE Department, Barcelona Supercomputing Center, Barcelona, Spain
[2]Istituto Nazionale di Geofisica e Vulcanologia, Sezione di Bologna, Italy
[3]Istituto Nazionale di Geofisica e Vulcanologia, Sezione di Napoli, Italy

Correspondence to: Arnau Folch (arnau.folch@bsc.es)

Abstract. Eruption Source Parameters (ESP) characterizing volcanic eruption plumes are crucial inputs for atmospheric tephra dispersal models, used for hazard assessment and risk mitigation. We present FPLUME-1.0, a steady-state 1D cross-section averaged eruption column model based on the Buoyant Plume Theory (BPT). The model accounts for plume ~~bent over~~ bending by wind, entrainment of ambient moisture, effects of water phase changes, particle fallout and re-entrainment, a new parameterization for the air entrainment coefficients and a model for wet aggregation of ash particles in presence of liquid water or ice. In the occurrence of wet aggregation, the model predicts an ~~"effective"~~ "effective" grain size distribution depleted in fines with respect to that erupted at the vent. Given a wind profile, the model can be used to determine the column height from the eruption mass flow rate or vice-versa. The ultimate goal is to improve ash cloud dispersal forecasts by better constraining the ESP (column height, eruption rate and vertical distribution of mass) and the ~~"effective"~~ "effective" particle grain size distribution resulting from eventual wet aggregation within the plume. As test cases we apply the model to the eruptive phase-B of the 4 April 1982 El Chichón volcano eruption (México) and the 6 May 2010 Eyjafjallajökull eruption phase (Iceland). The modular structure of the code facilitates the implementation in the future code versions of more quantitative ash aggregation parameterization as further observations and experiments data will be available for better constraining ash aggregation processes.

1 Introduction

Volcanic plumes (e.g. Sparks, 1997) are ~~a~~ turbulent multiphase flows containing volcanic gas, entrained ambient air and moisture and ~~suspended~~ tephra, consisting on both juvenile (resulting from magma fragmentation), crystal and lithic (resulting from wall rock erosion) particles ranging from

meter-sized blocks to micron-sized fine ash (diameter $\leq 63\mu m$). Sustained volcanic plumes present a ~~basal jet~~ negatively buoyant basal thrust region where the mixture rises due to its momentum. As ambient air is entrained by turbulent mixing, it heats and expands, thereby reducing the average density of the mixture. It leads to a transition to the convective region, in which positive buoyancy drives the mixture ~~upwards above~~ up to the so-called Neutral Buoyancy Level (NBL), where the mixture density equals that of the surrounding atmosphere. ~~For strong plumes, excess~~ Excess of momentum above the NBL (overshooting) can ~~effectively~~ drive the mixture higher forming the umbrella region, where tephra disperses horizontally first as a gravity current ~~(e.g. Costa et al., 2013)~~ (e.g. Costa et al., 2013; Carazzo et al., 2014) and then under passive wind advection forming a volcanic cloud (see Fig. 1). ~~Depending on the balance between the ascending plume velocity and the height-dependent horizontal wind velocity, plumes can rise sub-vertically (strong plumes) or bent-over spreading laterally around the NBL, often without developing an umbrella region (weak plumes).~~

~~Characterization trough observations and monitoring and modeling~~ Quantitative observations and models of volcanic plumes ~~is~~ are essential to provide realistic source terms to atmospheric dispersal models, aimed at simulating atmospheric tephra transport and/or the resulting fallout deposit (e.g. Folch, 2012). Plume models range in complexity from 1D ~~integrated models build~~ integral models built upon the Buoyant Plume Theory (BPT) of Morton et al. (1956) to sophisticated multiphase Computational Fluid Dynamics (CFD) models (e.g. Suzuki et al., 2005; Esposti Ongaro et al., 2007; Suzuki and Koyaguchi, 2009; Herzog and Graf, 2010; Suzuki and Koyaguchi, 2013). The latter group of models are valuable to understand physical phenomena and the role of different parameters but, given ~~its~~ their high computational cost, coupling with atmospheric dispersal models at an operational level is still unpractical. Moreover even sophisticated 3D multiphase models can have serious problems to accurately describe the physical processes related to e.g. closure equations, computational spatial resolution, etc. For this reason, simpler 1D cross-section averaged models or even empirical relationships between plume height and eruption rate (e.g. Mastin et al., 2009; Degruyter and Bonadonna, 2012) are used in practice to furnish Eruption Source Parameters (ESP) to atmospheric transport models, the results of which strongly depend on the source term quantification (*i.e.* determination of plume height, eruption rate, vertical distribution of mass and particle grain size distribution).

Many plume models based on the BPT have been proposed after the seminal studies of Wilson (1976) and Sparks (1986) to address different aspects of plume dynamics. For example, ~~?Woods (1993)~~ Woods (1993) proposed a model to include the latent heat associated with condensation of water ~~vapor~~ vapour and quantify its effects upon the eruption column. Ernst et al. (1996) presented a model considering particle sedimentation and re-entrainment from plume margins. Bursik (2001) analyzed how the interaction with wind enhances entrainment of air, plume bending, and decrease of the total plume height for a given eruption rate. Several other plume models exist ~~(e.g. ?Degruyter and Bonadonna, 2012; Woodhouse et al., 2013; Devenish, 2013; de~~ considering different modelling approaches, simplifying assumptions and model parameterizations.

It is well recognized that the values of the air entrainment coefficients have a large influence on the results of the plume models. On the other hand, volcanic ash aggregation (e.g. Brown et al., 2012) can occur within the eruption column or, under certain circumstances, downstream within the ash cloud (Durant et al., 2009). In any case, the formation of ash aggregates (with typical sizes around few hundreds of μm and less ~~denser~~ dense than the primary particles) dramatically impacts particle transport dynamics thereby reducing the atmospheric residence time of aggregating particles and promoting the premature fallout of fine ash. As a result, atmospheric transport models neglecting aggregation tend to overestimate far-range ash cloud concentrations, leading to an overestimation of the risk posed by ash clouds on civil aviation and an underestimation of ash loading in the near field. So far, no plume model tries to predict the formation of ash aggregates in the eruptive column and how it affects the particle grain size distribution erupted at the vent. This can be explained in part because aggregation mechanisms are complex and not fully understood yet, although theoretical models have been proposed for wet aggregation (Costa et al., 2010; Folch et al., 2010).

Here we present FPLUME-1.0, a steady-state 1D cross-section averaged plume model which accounts for plume ~~bent over~~bending, entrainment of ambient moisture, effects of water phase changes on the energy budget, particle fallout and re-entrainment by turbulent eddies, variable entrainment coefficients fitted from experiments, and particle aggregation in presence of liquid water or ice that depends on plume dynamics, particle properties, and amount of liquid water and ice existing in the plume. The ~~modeling~~ modelling of aggregation in the plume, proposed here for the first time, allows our model to predict an "effective" Total Grain Size Distribution (TGSD) depleted in fines with respect to that erupted at the vent. The ultimate goal is to improve ash cloud forecasts by better constraining ~~this relevant aspect~~ these relevant aspects of the source term. In this manuscript, we present first the governing equations for the plume and aggregation models and then apply the combined model to two test cases, the eruptive phase-B of the 1982 El Chichón volcano eruption (México) and the 6 May 2010 Eyjafjallajökull eruption phase (Iceland).

2 Physical Plume Model

We consider a volcanic plume as a multiphase mixture of volatiles, suspended particles (tephra) and entrained ambient air. For simplicity, water (in ~~vapor~~vapour, liquid or ice phase) is assumed the only volatile ~~specie~~species, being either of magmatic origin or incorporated trough the ingestion of moist ambient air. Erupted tephra particles can form by magma fragmentation or by erosion of the volcanic conduit, and can vary notably in size, shape and density. For historical reasons, field volcanologists describe the continuous spectrum of particle sizes in terms of the dimensionless Φ-scale (Krumbein, 1934):

$$d(\Phi) = d_* 2^{-\Phi} = d_* e^{-\Phi \log 2} \tag{1}$$

where d is the particle size and $d_* = 10^{-3}\mathrm{m}$ is a reference length (*i.e.* $2^{-\Phi}$ is the direction-averaged particle size expressed in mm). The vast majority of ~~modeling~~ modelling strategies, discretize the continuous particle Grain Size Distribution (GSD) by grouping particles in n different Φ-bins, each with an associated particle mass fraction (the models based on moments (e.g. de' Michieli Vitturi et al., 2015) are the exception). Because particle size exerts a primary control on sedimentation, Φ-classes are often identified with terminal settling velocity classes although, strictly, a particle settling velocity class is ~~univocally~~ defined not only by particle size but also by its density and shape. We propose a model for volcanic plumes as a multiphase homogeneous mixture of water (in any phase), entrained air, and n particle classes, including a parameterization for the air entrainment coefficients and a wet aggregation model. Because the governing equations based upon the BPT are not adequate above NBL, we also propose a new semi-empirical model to describe such a region.

2.1 Governing Equations

The steady-state cross-section averaged governing equations for axisymmetric plume motion in a turbulent wind ~~are~~ (see Fig. 1) are the following (for the meaining of the used symbols see Tables 1 and 2):

$$\frac{d\hat{M}}{ds} = 2\pi r \rho_a u_e + \sum_{i=1}^{n} \frac{d\hat{M}_i}{ds} \tag{2a}$$

$$\frac{d\hat{P}}{ds} = \pi r^2 \left(\rho_a - \hat{\rho}\right) g \sin\theta + u_a \cos\theta \left(2\pi r \rho_a u_e\right) + \hat{u} \sum_{i=1}^{n} \frac{d\hat{M}_i}{ds} \tag{2b}$$

$$\hat{P}\frac{d\theta}{ds} = \pi r^2 \left(\rho_a - \hat{\rho}\right) g \cos\theta - u_a \sin\theta \left(2\pi r \rho_a u_e\right) \tag{2c}$$

$$\frac{d\hat{E}}{ds} = 2\pi r \rho_a u_e \left((1 - w_a) c_a T_a + w_a h_{wa}(T_a) + gz + \frac{1}{2} u_e^2 \right) + c_p \hat{T} \sum_{i=1}^{n} \frac{d\hat{M}_i}{ds} + L_c \frac{d}{ds}_l + L_d \frac{d}{ds}_s \tag{2d}$$

$$\frac{d\hat{M}_a}{ds} = 2\pi r \rho_a u_e (1 - w_a) \tag{2e}$$

$$\frac{d\hat{M}_w}{ds} = 2\pi r \rho_a u_e w_a \tag{2f}$$

$$\frac{d\hat{M}_i}{ds} = \frac{\chi}{r\hat{u}} \frac{\chi u_{si}}{r\hat{u}} \left(\frac{f u_e}{dr/ds} - u_{si} 1 + \frac{f u_e}{u_{si} dr/ds} \right)^{-1} \hat{M}_i + A_i^+ - A_i^- \tag{2g}$$

$$\frac{dx}{ds} = \cos\theta \cos\Phi_a \tag{2h}$$

$$\frac{dy}{ds} = \cos\theta \sin\Phi_a \tag{2i}$$

$$\frac{dz}{ds} = \sin\theta \tag{2j}$$

where $\hat{M} = \pi r^2 \hat{\rho} \hat{u}$ is the total mass flow rate, $\hat{P} = \hat{M}\hat{u}$ is the total axial (stream-wise) momentum flow rate, θ is the plume bent over angle with respect to the horizontal (*i.e.* $\theta = 90°$ for a plume raising vertically), $\cancel{\hat{E} = \hat{M}(\hat{c}\hat{T} + gz + \frac{1}{2}\hat{u}^2)}$ $\hat{E} = \hat{M}(\hat{H} + gz + \frac{1}{2}\hat{u}^2)$ is the total energy flow rate, $\hat{H}$ is the enthalpy flow rate of the mixture, $\hat{T} = \hat{T}(\hat{H})$ is the mixture temperature, $\hat{M}_a$ is the mass flow rate of dry air, $\hat{M}_w = \hat{M}\hat{x}_w$ is the mass flow rate of volatiles (including water ~~vapor~~vapour, liquid and ice), h_{wa} is the enthalpy per unit mass of the water in the atmosphere, $\hat{M}_i = \hat{M}\hat{x}_p f_i$ is the mass flow rate of particles of class $i (i = 1 : n)$, x and y are the horizontal coordinates, z is height, and s is the distance along the plume axis (see Tables 1 and 2 for the definition of all symbols and variables appearing in the manuscript).

The equations above derive from conservation principles assuming axial (stream-wise) symmetry and considering bulk quantities integrated over a plume cross-section using a top-hat profile in which a generic quantity ϕ has a constant value $\hat{\phi}(s)$ at a given plume cross-section and vanishes outside (here we refer to section-averaged quantities as ~~"bulk "~~ bulk quantities, denoted by a hat). We have derived these equations by combining formulations from different previous plume models (Netterville, 1990; Woods, 1993; Ernst et al., 1996; Bursik, 2001; Costa et al., 2006; Woodhouse et al., 2013) in order to include in a single model effects from plume ~~bent over~~ bending by wind, particle fallout and re-entrainment at plume margins, transport of volatiles (water) accounting also for ingestion of ambient moisture, phase changes (water ~~vapor~~ vapour condensation and deposition) and particle aggregation. Equation (2a) expresses the conservation of total mass, accounting in the Right Hand Side (RHS) for the mass of air entrained through the plume margins and the loss/gain of mass by particle fallout/re-entrainment. Equations (2b) and (2c) express the conservation of axial (stream-wise) and radial momentum respectively, accounting ~~in~~ on the RHS for contributions from buoyancy (first term), entrainment of air, and particle fallout/re-entrainment. Note that generally the buoyancy term, acting only along the vertical direction z, ~~acts as~~ represents a sink of momentum in the basal gas-thrust jet region (where $\hat{\rho} > \rho_a$) and ~~as~~ a source of momentum where the plume is positively buoyant ($\hat{\rho} < \rho_a$). Equation (2d) express the conservation of energy, accounting ~~in~~ on the RHS for gain of energy (enthalpy, potential and kinetic) by ambient air entrainment (first term), loss/gain by particle fallout/re-entrainment (second term), and gain of energy by conversion of water ~~vapor~~ vapour into liquid (condensation) or into ice (deposition). Equations (2e), (2f) and (2g)

express, respectively, the conservation of mass of dry air, water (~~vapor~~vapour, liquid and ice) and solid particles. The latter set of equations, one for each particle class, account ~~in~~ on the RHS for particle re-entrainment (first term), particle fallout (second term) and particle aggregation. Here we have included to terms (A_i^+ and A_i^-) that account for the creation of mass from smaller particles aggregating into particle class i and for the destruction of mass resulting from particles of class i contributing to the formation of larger-size aggregates. Finally, Eqs. (2h) to (2j) determine the 3D plume trajectory as a function of the length parameter s. All these equations constitute a set of $9+n$ first order ordinary differential equations in s for $9+n$ unknowns: $\hat{M}$, $\hat{P}$, θ, $\hat{E}$, $\hat{M}_a$, $\hat{M}_w$, $\hat{M}_i$ (for each particle class), x, y and z. Note that, using the definitions of $\hat{M}$-$\hat{P}$-$\hat{E}$, the equations can also be expressed in terms of $\hat{u}$-r-$\hat{T}$ given the bulk density.

Assuming an homogeneous mixture, the bulk density $\hat{\rho}$ of the mixture is:

$$\frac{1}{\hat{\rho}} = \frac{\hat{x}_p}{\rho_p} + \frac{\hat{x}_l}{\rho_l} + \frac{\hat{x}_s}{\rho_s} + \frac{(1-\hat{x}_p-\hat{x}_l-\hat{x}_s)}{\rho_g} \tag{3}$$

where $\hat{x}_p$, $\hat{x}_l$ and $\hat{x}_s$ are, respectively, the mass fractions of particles, liquid water and ice, ρ_p is the ~~class-averaged particle~~ class-weighted average density of particles (pyroclasts)~~density~~, ρ_l and ρ_s are liquid water and ice densities, and ρ_g is the gas phase (*i.e.* dry air plus water ~~vapor~~vapour) density. ~~We assume that $\rho_g \approx \rho_a(\hat{T})$ where ρ_a is the air density (at the bulk temperature).~~ Under the assumption of mechanical equilibrium (*i.e.* assuming the same bulk velocity $\hat{u}$ for all phases and components) is holds that:

$$\hat{x}_p = \frac{\sum \hat{M}_i}{\hat{M}} = \frac{\sum \hat{M}_i}{\sum \hat{M}_i + \hat{M}_w + \hat{M}_a} \tag{4}$$

~~Additional hypothesis arenecessary in order to determine how the mass fraction of water~~ The enthalpy flow rate of the mixture is a non-decreasing function of the temperature $\hat{T}$, given by:

$$\hat{H} = \hat{M}[x_a c_a \hat{T} + x_p c_p \hat{T} + x_v h_v(\hat{T}) + x_l h_l(\hat{T}) + x_s h_s(\hat{T})] \tag{5}$$

where h_v, h_l, and h_s are, respectively, the enthalpy per unit mass of water vapour, liquid, and ice:

$$h_s(\hat{T}) = c_s \hat{T} \tag{6a}$$

$$h_l(\hat{T}) = h_{l0} + c_l(\hat{T} - T_0) \tag{6b}$$

$$h_v(\hat{T}) = h_{v0} + c_v(\hat{T} - T_0) \tag{6c}$$

where $c_s = 2108\,\mathrm{J\,K^{-1}kg^{-1}}$ is the specific heat of ice, T_0 is a reference temperature, $h_{l0} = 3.337\times10^5\,\mathrm{J\,kg^{-1}}$ is the enthalpy of the liquid water at the reference temperature, $c_l = 4187\,\mathrm{J\,K^{-1}kg^{-1}}$ is the specific

heat of liquid water, $h_{v0} = 2.501 \times 10^6$ J kg^{-1} is the enthalpy of vapour water at the reference temperature and $c_v = 1996$ J K^{-1}kg^{-1} is the specific heat of vapour water. For convenience, the reference temperature T_0 is taken equal to the temperature of triple point of the water ($T_0 = 273.15$ K). The energy and the enthalpy flow rate are related by:

$$\hat{E} = \hat{H} + \hat{M}(gz + \frac{1}{2}u^2) \tag{7}$$

For the integration of Eq.(2d) and for evaluating the aggregation rate terms in Eq.(2g), the temperature $\hat{T}$ and the mass fractions of ice (x_s), liquid water (~~$\hat{x}_w = \hat{x}_v + \hat{x}_l + \hat{x}_s$) distributes amongst the different phases depending on temperature~~x_l) and vapour (x_v) need to be evaluated. These quantities are obtained by the direct inversion of Eq.(5), with the use of eqs.(2d) and (7) and by assuming that the pressure inside the plume P is equal to the atmospheric pressure at the same altitude (z).

The model uses a pseudo-gas assumption considering that the mixture of air and water vapour behaves as an ideal gas:

$$P = P_v + P_a \; ; \qquad P_v = n_v P \; ; \qquad P_a = n_a P \tag{8a}$$

$$n_v = \frac{x_v/m_v}{x_v/m_v + x_a/m_a} \; ; \qquad n_a = \frac{x_a/m_a}{x_v/m_v + x_a/m_a} \tag{8b}$$

where P_v and ~~pressure. As in Folch et al. (2010), we consider the existence of a freezing temperature (T_f)below which all liquid water~~ P_a are, respectively the partial pressures of the water vapour and of the air in the plume, n_v and ~~vapor in excess (if any) are converted instantaneously to ice (i.e.the three water phases do not coexist in any section of the plume). In addition, and following~~ n_a are the molar fractions of vapour and air in the gas phase ($n_v + n_a = 1$) and $m_v = 0.018$ kg/mole and $m_a = 0.029$ kg/mole are the molar weights of vapour and air. Following Woods (1993) and Woodhouse et al. (2013), we ~~also~~ consider that, if the air-water mixture becomes saturated in water ~~vapor~~vapour, condensation or deposition ~~occur rapidly~~ occurs and the plume remains just saturated. This assumption implies that the partial pressure of water ~~vapor~~ vapour P_v ~~:~~

$$P_v = \frac{\hat{M}\hat{x}_v}{\hat{M}_a + \hat{M}\hat{x}_v} P$$

equals the saturation pressure of ~~vapor~~ vapour over liquid (e_l) or over ice (e_s) at the bulk temperature, ~~where P is pressure (approximated to the atmospheric pressure at a given height, $P \approx P_a(z)$)~~ and the saturation pressures over liquid and ice are given (in hPa) by (Murphy and Koop, 2005):

$$e_l = 6.112 \exp\left(17.67 \frac{\hat{T} - 273.16}{\hat{T} - 29.65}\right) \tag{9}$$

$$\log e_s = -9.097(\frac{273.16}{\hat{T}} - 1) - 3.566 \log(\frac{273.16}{\hat{T}}) + 0.876(1 - \frac{\hat{T}}{273.16}) + \log(6.1071) \tag{10}$$

Equation (9) holds for $\hat{T} > T_f$ and Eq. (10) is valid for $\hat{T} < T_f$, where T_f is the temperature of the triple point of the water (here set at $P_f = 611.2$ Pa, $T_f = 273.16$ K). Therefore, if $\hat{T} > T_f$ and $P_v < e_l$ the plume is undersaturated and there is no water ~~vapor~~ vapour condensation (*i.e.* $\hat{x}_v = \hat{x}_w$ and $\hat{x}_l = \hat{x}_s = 0$). In contrast, if $P_v \geq e_l$, the ~~vapor~~ vapour in excess is immediately converted into liquid and:

$$(P - e_l)\, n_v = \frac{e_l}{P - e_l}\frac{\hat{M}_a}{\hat{M}} = \frac{e_l}{P - e_l}\frac{\hat{M}_a}{\sum \hat{M}_i + \hat{M}_w + \hat{M}_a} e_l\, n_a$$

$$\hat{x}_s = 0$$

$$\hat{x}_l = \hat{x}_w - \hat{x}_v = \frac{\hat{M}_w}{\sum \hat{M}_i + \hat{M}_w + \hat{M}_a} - v$$

(11)

The vapour and air mass fractions x_v and x_a are evaluated by combining Eq.(11) and (8b). On the other hand, if $\hat{T} \leq T_f$ and $P_v < e_s$ the plume is undersaturated and there is no water ~~vapor~~ vapour deposition. In contrast, if $P_v \geq e_s$, the ~~vapor~~ vapour in excess is immediately converted into ice and:

$$(P - e_s)\, n_v = \frac{e_s}{P - e_s}\frac{\hat{M}_a}{\hat{M}} = \frac{e_s}{P - e_s}\frac{\hat{M}_a}{\sum \hat{M}_i + \hat{M}_w + \hat{M}_a} e_s\, n_a$$

$$\hat{x}_l = 0$$

$$\hat{x}_s = \hat{x}_w - \hat{x}_v = \frac{\hat{M}_w}{\sum \hat{M}_i + \hat{M}_w + \hat{M}_a} - v$$

(12)

~~The latent heat released by water vapor condensation and deposition can provide an important additional source of energy for small to moderate plumes in moist environments (Woods, 1993) and is given by:~~ Again, the vapour and air mass fractions x_v and x_a are evaluated by combining Eq.(12) and (8b).

$$L_c = L_{co} + (c_v - c_l)(\hat{T} - T_o)$$

$$L_d = L_{do} + (c_v - c_s)(\hat{T} - T_o)$$

~~where $L_{co} = 2.50 \times 10^6$ and $L_{do} = 2.83 \times 10^6$ are the latent heats of condensation and deposition at $T_o = 273$K. Assuming thermal equilibrium between water phases, air and particles, the specific heat capacity of the mixture $\hat{c}$ is given by :~~

$$\hat{c} = \frac{c_p \sum \hat{M}_i + (c_v \hat{x}_v + c_l \hat{x}_l + c_s \hat{x}_s)\hat{M}_w + c_a \hat{M}_a}{\sum \hat{M}_i + \hat{M}_w + \hat{M}_a}$$

For the particle re-entrainment parameter f we adopt the fit proposed by Ernst et al. (1996) using data for plumes not affected by wind:

$$f = 0.43\left(1 + \left[\frac{0.78 u_s P_o^{1/4}}{F_o^{1/2}}\right]^6\right)^{-1} \tag{13}$$

where $P_o = r_o^2 \hat{u}_o^2$ and $\cancel{F_o = r_o^2 \hat{u}_o \hat{c}_o \hat{T}_o}$ $F_o = r_o^2 \hat{u}_o \hat{H}_o$ are the specific momentum and thermal fluxes at the vent ($\cancel{s = 0)}$$s = 0$), and $\hat{H}_o$ is the enthalpy per unit mass of the mixture at the vent. This expression may overestimate re-entrainment for bent over plumes (Bursik, 2001). Finally, particle terminal settling velocity u_{si} is parameterized as (Costa et al., 2006; Folch et al., 2009):

$$u_{si} = \sqrt{\frac{4g(\rho_{pi} - \hat{\rho})d_i}{3C_d\hat{\rho}}} \tag{14}$$

where d_i is the class particle diameter and C_d is a drag coefficient that depends on the Reynolds number $Re = d_i u_{si}\hat{\rho}/\hat{\mu}$. Several empirical fits exist for drag coefficients of spherical and non-spherical particles (e.g. Wilson and Huang, 1979; Arastoopour et al., 1982; Ganser, 1993; Dellino et al., 2005). In particular, Ganser (1993) gives a fit valid over a wide range of particle sizes and shapes covering the spectrum of volcanic particles considered in volcanic column models (lapilli and ash):

$$C_d = \frac{24}{ReK_1}\left\{1 + 0.1118[Re(K_1K_2)]^{0.6567}\right\} + \frac{0.4305K_2}{1 + \frac{3305}{ReK_1K_2}} \tag{15}$$

where K_1 and K_2 are two shape factors depending on particle sphericity, Ψ, and particle orientation. Given that the C_d depends on Re (*i.e.* on u_s), Eq. 14 is solved iteratively using a bisection algorithm. Given a closure equation for the turbulent air entrainment velocity u_e, and an aggregation model (defining the mass aggregation coefficients A_i^+ and A_i^-), Eqs. (2a) to (2i) can be integrated along the plume axis from the inlet (volcanic vent) up to the neutral buoyancy level. Inflow (boundary) conditions are required at the vent ($s = 0$) for, *e.g.*, total mass flow rate $\hat{M}_o$, bent over angle $\theta_o = 90°$, temperature $\hat{T}_o$, exit velocity $\hat{u}_o$, fraction of water $\hat{x}_{wo}$, null air mass flow rate $\hat{M}_a = 0$, vent coordinates (x_o,y_o and z_o), and mass flow rate for each particle class $\hat{M}_{io}$. The latter is obtained from the total mass flow rate at inflow given the particle grain size distribution at the vent:

$$\hat{M}_{io} = f_{io}\hat{M}_o(1 - \hat{x}_{wo}) \tag{16}$$

where f_{io} is the mass fraction of class i at the vent.

2.2 Entrainment coefficients

Turbulent entrainment of ambient air plays a key role on the dynamics of jets and buoyant plumes. In the basal region of volcanic columns, the rate of entrainment dictates ~~if~~ whether the volcanic jet enters into a collapse regime by exhaustion of momentum before the mixture becomes positively buoyant or ~~if~~ whether it evolves into a convective regime reaching much higher altitudes. Early

laboratory experiments (e.g. Hewett et al., 1971) already indicated that the velocity of entrainment of ambient air is proportional to velocity differences parallel and normal to the plume axis (see inset in Fig. 1):

$$u_e = \alpha_s|\hat{u} - u_a\cos\theta| + \alpha_v|u_a\sin\theta| \tag{17}$$

where α_s and α_v are dimensionless coefficients that control the entrainment along the stream-wise (shear) and cross-flow (vortex) directions respectively. Note that, in absence of wind (*i.e.* $u_a = 0$), the equation above reduces to $u_e = \alpha_s\hat{u}$ and the classical expression for entrainment velocity of Morton et al. (1956) is recovered. In contrast, under a wind field, both an along-plume (proportional to the relative velocity differences parallel to the plume) and a cross-flow (proportional to the wind normal component) contributions appear. However it is worth noting that Eq. (17) has not a solid theoretical justification and is used on empirical basis. A vast literature exists regarding the experimental (e.g. Dellino et al., 2014) and numerical (e.g. Suzuki and Koyaguchi, 2009) determination of entrainment coefficients for jets and buoyant plumes. Based on these results, most 1D ~~integrated~~ integral plume models available in literature consider: i) same constant entrainment coefficients along the plume, ii) pice-wise constant values at the different regions or, iii) pice-wise constant values corrected by a factor $\sqrt{\hat{\rho}/\rho_a}$ (Woods, 1993). Typical values for the entrainment coefficients derived from experiments are of the order of $\alpha_s \approx 0.07 - 0.1$ for the jet region, $\alpha_s \approx 0.1 - 0.17$ for the buoyant region, and $\alpha_v \approx 0.3 - 1.0$ (e.g. Devenish, 2013). However, more recent experimental (Kaminski et al., 2005) and sensitivity analysis numerical studies (Charpentier and Espíndola, 2005) concluded that pice-wise constant functions are valid only as a first approach, implying that 1D ~~integrated~~ integral models assuming constant entrainment coefficients do not always provide satisfactory results. This has also been corroborated by 3D numerical simulations of volcanic plumes (Suzuki and Koyaguchi, 2013), which indicate that 1D ~~integrated~~ integral models overestimate the effects of wind on turbulent mixing efficiency (*i.e.* the value of α_v) and, consequently, underestimate plume heights under strong wind fields. For example, recent 3D numerical simulation results for small-scale eruptions under strong wind fields suggest lower values of α_v, in the range $0.1 - 0.3$ (Suzuki and Koyaguchi, 2015). ~~Based on experimental studies,~~ For this reason, besides the option of constant entrainment coefficients, FPLUME allows considering also a parameterization of α_s and α_v based on the local Richardson number. In particular, we use the empirical parameterization of Kaminski et al. (2005) and Carazzo et al. (2006, 2008a, b) ~~proposed a parameterization for the shear entrainment coefficient~~ that describes α_s ~~of~~ for jets and plumes as a function of the local Richardson number as:

$$\alpha_s = 0.0675 + \left(1 - \frac{1}{A(z_s)}\right) Ri + \frac{r}{2}\frac{1}{A(z_s)}\frac{dA}{dz} \tag{18}$$

where $A(z_s)$ is an entrainment function depending on the dimensionless length $z_s = z/2r_o$ (r_o is the vent radius) and $Ri = g(\rho_a - \hat{\rho})r/\rho_a\hat{u}^2$ is the Richardson number. ~~In order to generalize to the case of two entrainment coefficient we modify such expression~~ Beside the local Richardson number, the

entrainment coefficient α_s depends on plume orientation (e.g. Lee and Cheung, 1990; Bemporad, 1994), therefore we modify Eq. 18 as:

$$\alpha_s = 0.0675 + \left(1 - \frac{1}{A(z_s)}\right) Ri \, \sin\theta + \frac{r}{2}\frac{1}{A(z_s)}\frac{dA}{dz} \tag{19}$$

Moreover in order to use a compact analytical expression and extend it to values of $z_s \leq 10$ we fitted the experimental data of Carazzo et al. (2006, 2008b) considering the following empirical function:

$$A(z_s) = c_o \frac{(z_s^2 + c_1)}{(z_s^2 + c_2)} \tag{20a}$$

$$\frac{1}{A(z_s)}\frac{dA}{dz} = \frac{1}{2r_0}\frac{2\,(c_2 - c_1) z_s}{(z_s^2 + c_1)\,(z_s^2 + c_2)} \tag{20b}$$

and in order to extrapolate to low z_s we multiply $A(z_s)$ for the following function $h(z_s)$ that affects the behavior only for small values of z_s:

$$h(z_s) = \frac{1}{1 - c_4 \exp\left(-5\,(z_s/10 - 1)\right)} \tag{20c}$$

where c_i are dimensionless fitting constants. Best-fit results and entrainment functions resulting from fitting Eqs. (20a)-(20c) are shown in Table 3 and Fig. 2 respectively. However, the veracity of the empirical parameterization in Eq. (18) was not observed by Wang and Wing-Keung Law (2002) in their experiments nor has it been seen in DNS or LES simulations of buoyant plumes (e.g. Craske et al., 2015). Finally, for the vortex entrainment coefficient α_v, we adopt a parameterization proposed by Tate (2002) based on a few laboratory experiments:

$$\alpha_v = 0.34\left(\sqrt{2|Ri|}\frac{\bar{u}_a}{\hat{u}_o}\right)^{-0.125} \tag{21}$$

where $\hat{u}_o$ is the mixture velocity at the vent and $\bar{u}_a$ is the average wind velocity. For illustrative purposes, Fig. 3 shows the entrainment coefficients α_s and α_v predicted by Eqs. (19) and (21) for weak and strong plume cases under a prescribed wind profile. It is important stressing that air entrainment rates play a first-order role on eruptive plume dynamics and a simple description in terms of entrainment coefficients, both assuming them as empirical constants or describing them like in (18), represents an over-simplication of the real physics characterizing the processes. A better quantification of entrainment rates is one of the current main challenges of the volcanological community (see Costa et al., 2015, and references therein).

2.3 ~~Modeling~~ Modelling of the Umbrella Region

The umbrella region is defined as the upper region of the plume, from about the NBL to the top of the column. This region can be dominated by ~~processes of collapse of the~~ fountaining processes of the eruptive mixture that reaches the top of the column, dissipating the excess of momentum at the

NBL, and then collapsing as a gravity current (e.g. Woods and Kienle, 1994; Costa et al., 2013). The 1-D BPT should not be extended to this region because it assumes that the mixture still entrains air with the same mechanisms ~~than~~ as below NBL and, moreover, predicts that the radius goes to infinity towards the top of the column. For these reasons, we describe the umbrella region adopting a simple semi-empirical approximation.~~We assume that~~

In the umbrella region ~~extends~~ (from the NBL to the top of the column~~. Moreover, we consider that in the umbrella region air entrainment is null and~~), we neglect air entrainment and assume that the mixture is homogeneous, *i.e.*~~-~~ the content of air, water vapour, liquid water, ice, and total mass of particles do not vary with z. Pressure $P(z)$ is ~~assumed~~ considered equal to the atmospheric pressure $P_a(z)$ evaluated at the same level, whereas temperature decreases with z due to the adiabatic cooling:

$$P(z) = P_a(z) \quad \text{and} \quad \frac{dT}{dP} = \frac{1}{\hat{c}\hat{\rho}} \tag{22}$$

As a consequence, the density of the mixture varies accordingly. The total height of the volcanic plume H_t, above the vent, is approximated as (e.g. Sparks, 1986):

$$H_t = 1.32 c_H (H_b + 8r_o) \tag{23}$$

where is a dimensionless parameter (typically $c_H = 1.32$), H_b is the height of the Neutral Buoyancy Level (above the vent) and r_o the radius at the vent. Between H_b and H_t, the coordinates x and y of the position of the plume centre and the plume radius r are parameterized as a function of the elevation z, with $H_b \leq z \leq H_t$. The position of the plume centre is assumed to vary linearly with the same slope at the NBL, whereas the effective plume radius is assumed to decrease as a Gaussian function:

$$x = x_b + (z - H_b) \left.\frac{dx}{dz}\right|_{z=z_b} \tag{24}$$

$$y = y_b + (z - H_b) \left.\frac{dy}{dz}\right|_{z=z_b} \tag{25}$$

$$r = r_b\, e^{-(z-H_b)^2/2\sigma_H^2} \tag{26}$$

where x_b, y_b, r_b are, respectively, the coordinates x and y of the center of the plume and the plume radius at the NBL, and $\sigma_H = H_t - H_b$.

Finally, assuming that the kinetic energy of the mixture is converted to potential energy, the vertical velocity is approximated to decrease as the square root of the distance from the NBL:

$$u_z = u_{zb} \sqrt{\frac{H_t - z}{H_t - H_b}} \tag{27}$$

where u_{zb} is the vertical velocity of the plume at the NBL.

Although the proposed empirical parameterization of the region above the NBL is qualitatively

consistent with the trends predicted by 3D numerical models (Costa et al., 2015), a more rigorous description requires further research.

3 Plume Wet Aggregation Model

Particle aggregation can occur inside the column or in the ash cloud during subsequent atmospheric dispersion (e.g. Carey and Sigurdsson, 1982; Durant et al., 2009), thereby affecting the sedimentation dynamics and deposition of volcanic ash. Our model explicitly accounts for aggregation in the plume by adding source (A_i^+) and sink (A_i^-) terms for aggregates and aggregated particles in their respective particle mass balance Eqs. (2g) and by modifying the settling velocity of ~~the~~ aggregates. Given the complexity of aggregation phenomena, not yet fully understood, we consider only the occurrence of wet aggregation and neglect dry aggregation mechanisms driven by electrostatic forces or disaggregation processes resulting from particle collisions that can break and decompose aggregates. Costa et al. (2010) and Folch et al. (2010) proposed a simplified wet aggregation model in which particles aggregate on a single effective aggregated class characterized by a diameter d_A (*i.e.* aggregation only involves particle classes having an effective diameter smaller than d_A, typically in the range 100-300 μm). ~~Under this simplifying~~ Obviously the assumption that all particles aggregate into a single particle class is simplistic and considering a range of aggregating classes would be more realistic. However, there are no quantitative data available for such a calibration. Hence, considering this assumption it follows that:

$$A_i^+ = \sum_{j=k+1}^{n} A_j^- \delta_{ik} \tag{28}$$

where k is the (given) index of the aggregated class and the sum over j spans all particle classes having diameters lower than d_A. The mass of particles of class i ($d_i < d_A$) that aggregate per unit of time and length in a given plume cross-section is:

$$A_i^- = \dot{n}_i \left(\rho_{pi} \frac{\pi}{6} d_i^3 \right) \pi r^2 \tag{29}$$

where $\dot{n}_i$ is the number of particles of class i that aggregate per unit volume and time, estimated as:

$$\dot{n}_i \approx \frac{\dot{n}_{tot} N_i}{\sum N_j} \tag{30}$$

In the expression above, N_i is the number of particles of diameter d_i in an aggregate of diameter d_A, and $\dot{n}_{tot}$ is the total particle decay per unit volume and time. Costa et al. (2010) considered that N_i is given by a semi-empirical fractal relationship (e.g. Jullien and Botet, 1987; Frenklach, 2002; Xiong and Friedlander, 2001):

$$N_i = k_f \left(\frac{d_A}{d_i} \right)^{D_f} \tag{31}$$

where k_f is a fractal pre-factor and D_f is the fractal exponent. Costa et al. (2010); Folch et al. (2010) assumed constant values for k_f and D_f that ~~where~~ were calibrated by best-fitting tephra deposits

from 18 May 1980 Mount St. Helens and 17-18 September 1992 Crater Peak eruptions. However, for the granulometric data from these deposits they used a cut-off considering only particles larger than about $10\mu\mathrm{m}$, for which the gravitational aggregation kernel dominates. This poses a problem if one wants to extend the granulometric distribution to include micrometric and sub-micrometric particles, for which the Brownian kernel is the dominant one (it is known that Brownian particle-particle interaction has typical values of $D_f \approx 2$, with values ranging between 1.5 and 2.5, *e.g.* Xiong and Friedlander (2001)). Actually, preliminary model tests involving micrometric and sub-micrometric particle classes considering constant values for D_f and k_f have revealed a strong dependency of results (fraction of aggregated mass) on both granulometric cut-off and bin width (particle grain size discretization). In order to overcome this problem, we assume a size-dependent fractal exponent as:

$$D_f(d) = D_{fo} - \frac{a\,(D_{fo} - D_{min})}{1 + \exp((d - d_\mu)/d_\mu)} \tag{32}$$

where $D_{fo} \leq 3$, $D_{min} = 1.6$, $d_\mu \approx 2\mu\mathrm{m}$, and $a = 1.36788$. The values of D_{min} and d_μ represent, respectively, the minimum value of D_f relevant for sub-micrometric particles and the scale below which the Brownian aggregation kernel becomes dominant. For the fractal pre-factor k_f we adopt the expression of Gmachowski (2002):

$$k_f = \left[\sqrt{1.56 - (1.728 - \frac{D_f}{2})^2} - 0.228\right]^{D_f} \left(\frac{2 + D_f}{D_f}\right)^{D_f/2} \tag{33}$$

Figure 4 shows the values of $D_f(d)$ and $k_f(d)$ predicted by Eqs. (32) and (33) for a range of D_{fo}. We have performed different tests to verify that, in this way, the results of the aggregation model become much more robust independently of the distribution cut-off ($\Phi_{min} = 8, 10, 12$) and bin width ($\Delta\Phi = 1, 0.5, 0.25$), with maximum differences in the aggregated mass laying always below 10%. The total particle decay per unit volume and time $\dot{n}_{tot}$ is given by:

$$\dot{n}_{tot} = \hat{f}\alpha_m(A_B n_{tot}^2 + A_{TI}\phi^{4/D_f} n_{tot}^{2-4/D_f} + A_S\phi^{3/D_f} n_{tot}^{2-3/D_f} + A_{DS}\phi^{4/D_f} n_{tot}^{2-4/D_f}) \tag{34}$$

where α_m is a mean (class-averaged) sticking efficiency, ϕ is the solid volume fraction, n_{tot} is the total number of particles per unit of volume that can potentially ~~participate to the aggregation~~ aggregate and $\hat{f}$ is a correction factor that accounts for conversion from gaussian to top-hat formalism (see Appendix A for details). The expression above comes from integrating the collection kernel over all particle sizes, and involves the product of the (averaged) sticking efficiency times the collision frequency function accounting for Brownian motion (A_B), collision due to turbulence as a result of inertial effects (A_{TI}), laminar and turbulent fluid shear (A_S), and differential sedimentation (A_{DS}). The term A_B derives from the Brownian collision kernel $\beta_{B,ij}$ ~~(e.g. Costa et al., 2010)~~(Costa et al., 2010):

$$\beta_{B,ij} = \frac{2k_b\hat{T}}{3\hat{\mu}} \frac{(d_i + d_j)^2}{d_j d_j} \tag{35}$$

where k_b is the Boltzmann constant and $\hat{\mu}$ is the mixture dynamic viscosity ($\approx$ air viscosity at the bulk temperature $\hat{T}$). The term A_{TI} derives from the collision kernel due to turbulence as result of

inertial effects $\beta_{TI,ij}$ (e.g. Pruppacher and Klett, 1996; Jacobson, 2005):

$$\beta_{TI,ij} = \frac{\epsilon^{3/4}}{g\hat{\nu}^{1/4}} \frac{\pi}{4} (d_i + d_j)^2 |u_{sj} - u_{si}| \tag{36}$$

where $\hat{\nu}$ is the mixture kinematic viscosity and ϵ is the dissipation rate of turbulent kinetic energy, computed assuming the Smagorinsky-Lilly model:

$$\epsilon = 2\sqrt{2} k_s^2 \frac{\hat{u}^3}{r} \tag{37}$$

where $k_s \approx 0.1 - 0.2$ is the constant of Smagorinsky. The term A_S derives from the collision kernel due to laminar and turbulent fluid shear $\beta_{S,ij}$ ~~(e.g. Costa et al., 2010)~~(Costa et al., 2010):

$$\beta_{S,ij} = \frac{\Gamma_S}{6} (d_i + d_j)^3 \tag{38}$$

where Γ_S is the fluid shear, computed as:

$$\Gamma_S = \max\left(\left| \frac{d\hat{u}}{dr} \right|, \left(\frac{\epsilon}{\nu} \right)^{1/2} \right) \tag{39}$$

Finally, the term A_{DS} derives from the differential sedimentation collision kernel $\beta_{DS,ij}$ (e.g. Costa et al., 2010):

$$\beta_{DS,ij} = \frac{\pi}{4} (d_i + d_j)^2 |u_{si} - u_{sj}| \tag{40}$$

where u_{si} denotes the settling velocity of particle class i. Note that, with respect to the original formulation of Costa et al. (2010), using the same approach and approximation, we have included the additional term A_{TI} due to the turbulent inertial kernel that, thanks to the similarity between Eqs. (40) and (36), can be easily derived. Once these kernels are integrated, expressions for the terms in Eq. (34) yield:

$$A_B = -\frac{4 k_b \hat{T}}{3\hat{\mu}} \tag{41a}$$

$$A_S = -\frac{2}{3} \Gamma_S \xi^3 \tag{41b}$$

$$A_{DS} = -\frac{\pi(\rho_p - \hat{\rho}) g \xi^4}{48\hat{\mu}} \tag{41c}$$

$$A_{TI} = 1.82 \frac{\epsilon^{3/4}}{g\nu^{1/4}} A_{DS} \tag{41d}$$

where $\xi = d_j v_j^{-1/D_f}$ is the diameter to volume fractal relationship and v_j is the particle volume. Note that for spherical particles in the Euclidean space ($D_f = 3$) $v_j = \pi d_j^3/6$ and $\xi = (6/\pi)^{1/3}$.

The total number of particles per unit of volume available for aggregation is related to particle class mass concentration at each section of the plume $\hat{C}_j$ and can be estimated as (see Appendix B):

$$n_{tot} = \frac{1}{3\log 2}\sum_j \left(\frac{6\hat{C}_j}{\pi\Delta\Phi_j\rho_{pj}}\right)\left[\frac{1}{d_{aj}^3} - \frac{1}{d_{bj}^3}\right] \tag{42}$$

where d_{aj} and d_{bj} are the particle diameters of the limits of the interval j and:

$$\hat{C}_j = \hat{\rho}\frac{\hat{M}_j}{\hat{M}} \tag{43}$$

Finally, the class-averaged sticking efficiency α_m appearing in (34) is computed as:

$$\alpha_m = \frac{\sum_i\sum_j f_i f_j \alpha_{ij}}{\sum_i\sum_j f_i f_j} \tag{44}$$

where f_k is the particle class mass fraction, and α_{ij} is the sticking efficiency between the classes i and j. In presence of a pure ice phase we assume that ash particles stick as ice particles ($\alpha_m = 0.09$). In contrast, in presence of a liquid phase, the aggregation model considers:

$$\alpha_{ij} = \frac{1}{1 + (St_{ij}/St_{cr})^q} \tag{45}$$

where $St_{cr} = 1.3$ is the critical Stokes number, $q = 0.8$ is a constant, and St_{ij} is the Stokes number based on the binder liquid (water) viscosity:

$$St_{ij} = \frac{8\hat{\rho}}{9\mu_l}\frac{d_i d_j}{d_i + d_j}|u_i - u_j| \tag{46}$$

where

$$|u_i - u_j| = |u_{si} - u_{sj}| + \frac{8k_b\hat{T}}{3\hat{\mu}\pi d_i d_j} + \frac{2\Gamma_s(d_i + d_j)}{3\pi} \tag{47}$$

Obviously, our aggregation model requires the presence of water either in liquid or solid phases, *i.e.* aggregation will only occur in ~~these~~ those regions of the plume where water ~~vapor~~ vapour (of magmatic origin or entrained by moist air) meets condensation/deposition conditions (Costa et al., 2010; Folch et al., 2010). This depends on complex relationships between plume dynamics and ambient conditions. For high-intensity (strong) plumes having high values of $\hat{M}$, the condition $P_v \geq e_l$ when $\hat{T} > T_f$ is rarely ~~meet~~met, implying no formation of a liquid water window within the plume. Aggregation occurs in this case only at the upper parts of the column, under the presence of ice. In contrast, lower-intensity (weak) plumes having lower values of $\hat{M}$ can form a liquid water window if the term M_a dominates in Eq. (8a). However, this also depends on a complex balance between air entrainment efficiency, ambient moisture, plume temperature, height level, cooling rate and ambient conditions. Aggregation by liquid water is much favored under moist environments and by efficient air entrainment. Note that, keeping all eruptive parameters constant, the occurrence (or not) of wet aggregation by liquid water can vary with time depending on fluctuations of the atmospheric moisture and wind intensity along the day.

~~In summary, the solution of the aggregation model embedded in FPLUME-1.0 consists on the following steps: At each section of the plume, determine the water vapor condensation or deposition conditions depending on $\hat{T}$ and P_v using Eq. (11) or Eq. (12) respectively. In case of saturation or deposition, compute the class-averaged sticking efficiency α_m for liquid water or ice using Eq. (44). Estimate the total number of particles per unit of volume available for aggregation n_{tot} depending on $\hat{C}_j$ using Eq. (42). Compute the integrated aggregation kernels using Eq. (41a) to Eq. (41d). Compute the total particle decay per unit volume and time $\dot{n}_{tot}$ using Eq. (34) depending also on the solid volume fraction. Compute the number of particles of diameter d_i in an aggregate of given diameter d_A using Eq. (31) assuming size-dependent fractal exponent D_f and pre-factor k_f. Compute class particle decay $\dot{n}_i$ using Eq. (30). Finally, compute the mass sink term for each aggregating class A_i^- using Eq. (29) and the mass source term A_i^+ for the aggregated class using Eq. (28) to introduce these terms in the particle class mass balance equations Eqs. (2g).~~

4 FPLUME-1.0

We solve the model equations using FPLUME-1.0, a code written in FORTRAN90 that uses the LSODE library (Hindmarsh, 1980) to solve the set of first order ordinary differential equations. Model inputs are eruption start and duration (different successive eruption phases can be considered), vent coordinates (x_o,y_o) and elevation (z_o), conditions at the vent (exit velocity $\hat{u}_o$, magma temperature $\hat{T}_o$, magmatic water mass fraction $\hat{w}_o$, and total grain size distribution) and total column height H_t or mass eruption rate $\hat{M}_o$. The code has two solving modes. If $\hat{M}_o$ is given, the code solves directly for H_t. On the contrary, if H_t is given, the code solves iteratively for $\hat{M}$. Wind profiles can be furnished in different formats, including standard atmosphere, atmospheric soundings, and profiles extracted from meteorological re-analysis datasets. If the aggregation model is switched on, additional inputs are required including size and density of the aggregated class, aggregates settling velocity factor (to account for the decrease in settling velocity of aggregates due to increase in porosity), and fractal exponent for coarse particles D_{fo}. The rest of parameters (*e.g.* specific heats, the value of the constant χ for particle fallout probability, parameterization of the entrainment coefficients, etc.) have assigned default values but can be modified by the user using a configure file.

Model outputs include a text file with the results for each eruption phase giving values of all computed variables (*e.g.* $\hat{u}$, $\hat{T}$, $\hat{\rho}$, etc.) at different heights, and a file ~~given~~ giving the mass flow rate of each particle class that falls from the column at different heights (cross-sections). This file provides the phase-dependent source term, and hence serves to couple FPLUME with atmospheric dispersion models. In case of wet aggregation, the effective granulometry predicted by the aggregation model is also provided. The solution of the aggregation model embedded in FPLUME-1.0 consists on the following steps:

1. At each section of the plume, determine the water vapour condensation or deposition conditions depending on $\hat{T}$ and P_v using Eq. (11) or Eq. (12) respectively.

2. In case of saturation or deposition, compute the class-averaged sticking efficiency α_m for liquid water or ice using Eq. (44).

3. Estimate the total number of particles per unit of volume available for aggregation n_{tot} depending on $\hat{C}_j$ using Eq. (42).

4. Compute the integrated aggregation kernels using Eq. (41a) to Eq. (41d).

5. Compute the total particle decay per unit volume and time $\dot{n}_{tot}$ using Eq. (34) depending also on the solid volume fraction.

6. Compute the number of particles of diameter d_i in an aggregate of given diameter d_A using Eq. (31) assuming size-dependent fractal exponent D_f and pre-factor k_f.

7. Compute class particle decay $\dot{n}_i$ using Eq. (30).

8. Finally, compute the mass sink term for each aggregating class A_i^- using Eq. (29) and the mass source term A_i^+ for the aggregated class using Eq. (28) to introduce these terms in the particle class mass balance equations Eqs. (2g).

5 Test Cases

As we mentioned above, here we apply FPLUME to two eruptions relatively well characterized by previous studies. In particular we consider the strong plume formed during 4 April 1982 by El Chichón 1982 eruption (e.g. Sigurdsson et al., 1984; Bonasia et al., 2012) and the weak plume formed during the 6 May 2010 Eyjafjallajökull eruption (e.g. Bonadonna et al., 2011; Folch, 2012).

5.1 Phase-B El Chichón 1982 eruption

El Chichón volcano reawakened in 1982 with three significant Plinian episodes occurring during March 29th (phase A) and April 4th (phases B and C). Here we focus on the second major event, starting at 01:35 UTC on April 4th and lasting nearly 4.5h (Sigurdsson et al., 1984). Bonasia et al. (2012) used analytical (HAZMAP) and numerical (FALL3D) tephra transport models to reconstruct ground deposit observations for the three main eruption fallout units. Deposit best-fit inversion results for phase-B suggested column heights between 28 and 32 km (above vent level, a.v.l.) and a total erupted mass ranging between 2.2×10^{12} and 3.7×10^{12} kg. Considering a duration ~~on~~ of 4.5h, the resulting averaged mass eruption rates are between 1×10^8 and 2.3×10^8 kg/s. TGSD of phases B and C were estimated by Rose and Durant (2009) weighting by mass, by isopach volume and using

the Voronoi method. Bonasia et al. (2012) found that the reconstruction of the deposits is reasonably achieved taking into account the empirical Cornell aggregation parameterization (Cornell et al., 1983). In this simplistic approach, 50% of the 63-44 μm ash, 75% of the 44-31 μm ash and 100% of the less than 31 μm ash are assumed to aggregate as particles with a diameter of 200 μm and density of 200 kgm^{-3}. Note that here, as in previous studies (Folch et al., 2010), we use a modified version of Cornell et al. (1983) parameterization that assumes that 90% and not 100% of the particle smaller than 31 μm fall as aggregates.

We use this test case to verify whether FPLUME can reproduce results from these previous studies and the results of our aggregation model are, in this case, consistent with those of Cornell et al. (1983) parameterization. Input values for FPLUME are summarized in Table 4. We used the TGSD of Rose and Durant (2009) with 17 particle classes ranging from 64 mm ($\Phi = -6$) to 1μm ($\Phi = 10$). The wind profile has been obtained from the University of Wyoming soundings database (weather.uwyo.edu/upperair/sounding.html) for 4 April 1982 at 00UTC at the station number 76644 (lon=-89.65, lat=20.97). Figure 5 shows the wind profile and the FPLUME results for bulk velocity and plume radius. The model predicts a total plume height of 28 km (a.s.l.), a mass eruption rate of 2.7×10^8 $\mathrm{kg/s}$, and a total erupted mass of 4.4×10^{12} kg. These values are consistent but slightly higher than those from previous studies (Bonasia et al., 2012). Regarding the aggregation model, we did several sensitivity runs to look into the impact of the fractal exponent D_{fo} on the fraction of aggregates, ranging this parameter between 2.85 and 3.0 at 0.01 steps values (see Fig. 6). As anticipated in the original formulation (Costa et al., 2010; Folch et al., 2010), the results of the aggregation model are sensitive to this parameter. Values of $D_{fo} = 2.96$ fit very well the total mass fraction of aggregates predicted by Cornell but not the fraction of the aggregating classes (Fig. 7 ~~a~~b). In contrast, we find a more reasonable fit with $D_{fo} = 2.92$, although in this case the relative differences for the total mass fraction of aggregates are of about 15%, with our model under-predicting with respect to Cornell (Fig. 7~~b~~ a).

A clear advantage of a physical aggregation model of ash particles inside the eruption column, with respect an empirical parameterization like (Cornell et al., 1983), is that ~~allows to estimate~~ it allows estimating the fraction of very fine ash that escapes to aggregation processes and is transported distally within the cloud. As we mentioned above, based on the features of the observed deposits, Cornell et al. (1983) proposed that 100% of particles smaller than 31 μm fall as aggregates that is quite reasonable as most of fine ash falls prematurely. However assessing the small mass fraction of fine ash that escapes to aggregation processes is crucial for aviation risk mitigation and for comparing model simulations with satellite observations. For example, in the case of El Chichón 1982 eruption, for $D_{fo} = 2.92$, the model predicts that $\approx$ 10% of fine ash between 20 and 2 μm in diameter escapes to aggregation processes. This value is an order of magnitude larger than that estimated by Schneider et al. (1999) using TOMS and AVHRR but we need to consider that we do not account for dry aggregation that can be dominant for very fine particles.

5.2 6 May 2010 Eyjafjallajökull eruption phase

The infamous April-May 2010 Eyjafjallajökull eruption, that disrupted the European North Atlantic region airspace (e.g. Folch, 2012), was characterized by a very pulsating behavior, resulting on ~~a~~ nearly continuous production of weak plumes that oscillated ~~in~~ on height between 2 and 10 km (a.s.l.) ~~along~~ during the 39 day-long eruption (e.g. Gudmundsson et al., 2012). During 4-8 May, Bonadonna et al. (2011) performed in-situ observations of tephra accumulation rates and PLUDIX Doppler radar measurements of settling velocities at different locations which then used to determine erupted mass, mass eruption rates and grain size distributions. The authors estimated a TGSD representative of 30 min of eruption by combining ground-based grain-size observations (using a Voronoi tessellation technique) and ash mass retrievals (7-9Φ particles) from MSG-SEVIRI satellite imagery for 6 May between 11:00 and 11:30 UTC. On the other hand, they also report the in-situ observation of sedimentation of dry and wet aggregates falling as particle clusters and poorly structured and liquid accretionary pellets (AP1 and AP3 according to Brown et al. (2012) nomenclature). Bonadonna et al. (2011) did also grain-size analyses of collected aggregates using scanning electron microscope (SEM) images. The combination of all these data allowed them to determine how the original TGSD was modified by the formation of different types of aggregates (see Fig. 8). The total mass fraction of aggregates was estimated to be about 25% with aggregate sizes ranging between 1Φ (500 μm) and 4Φ (62.5 μm). These results constitute a rare and valuable dataset to test the aggregation model implemented in FPLUME. However, several challenges can be anticipated. First, our model assumes a single aggregated class and, as a consequence, we ~~can~~ may expect to reproduce only the total mass fraction of aggregates, but not to match the resulting mass fraction distribution class by class. Second, the proportion of dry versus wet aggregates is unknown and, ~~moreover,~~ wet aggregation could have occurred within the plume but also by local rain showers that scavenged coarse particles (Bonadonna et al., 2011), moreover the presence of meteoritic water in the plume (not considered here) could significantly enhance aggregation. For these reasons, we aim to capture the correct order of magnitude of total mass fraction of ash that went into aggregates.

~~Input values for FPLUME are summarized in Table 5. The wind profile (see Fig. 9) was extracted from the ERA-Interim re-analysis dataset interpolating values at the vent coordinates.~~ Preliminary simulations using time-averaged plume heights of 3.5-4.5 km (a.v.l.) did not result in formation of aggregates because the model did not predict the existence of a liquid water window nor the formation of ice. However, on short time scales these plume heights ~~can be~~ are very different from the daily (hourly) time-averaged values. In fact, Arason et al. (2011) determined 5-min time series of the echo top radar data of the eruption plume altitude and for 6 May they observed oscillations between 3.5 and 8.5 km (a.v.l). This is consistent with Gudmundsson et al. (2012), which for 6 May reported a median plume height of 4 km (a.v.l.) and a maximum elevation of around 8 km (a.v.l.). This may suggest that wet aggregates could have formed within the plume not continuously but during sporadic higher-intensity column pulses. In order to check this possibility, we performed a parametric

study to compute the total mass fraction of ~~formed wet aggregates depending on the~~ wet aggregates as function of mass flow rate that controls the value of the column height.

Input values for FPLUME are summarized in Table 5. The wind profile (see Fig. 9) was extracted from the ERA-Interim re-analysis dataset interpolating values at the vent coordinates. As shown in Fig. 10, 10% in mass of wet aggregates is predicted by our model ~~only~~ for column heights ranging between ~~6.7 and 7.5~~ 6 and 7 km (a.v.l.) ~~.~~ and 20% for column heights from 7.2 to 8.3 km (a.v.l.). For the considered input parameters ~~, model entrainment parameterizations,~~ and ambient conditions (wind and moisture profile), we ~~only~~ observed the formation of a window in the plume containing liquid water ~~for plume altitudes above 5.8~~ only for column heights above 5.3 km (a.v.l.). For illustrative purposes, Fig.11 shows the resulting grain size distribution for a column height of ~~7~~ 6.5 km (a.v.l.) and two different values of the fractal exponent D_f. As anticipated, the model can predict the total mass fraction of aggregates, but an error ($< 10\%$) exists for some particular classes. However, it should be kept in mind that mass fraction of aggregates is not controlled only by the eruptive column height but depends on several variables such as particle concentration (that is a function of the mass flow rate), presence of liquid water (that can form above a given level depending on the local meteorological conditions), etc.

6 Conclusions

We presented FPLUME, a 1D cross-section averaged volcanic plume model based on the BPT that accounts for plume ~~bent over~~ bending by wind, entrainment of ambient moisture, effects of water phase changes, particle fallout and re-entrainment, a new parameterization for the air entrainment coefficients and an ash wet aggregation model based on Costa et al. (2010). Given conditions at the vent (mixture exit velocity, temperature and magmatic water content) and a wind profile, the model can solve for plume height given the eruption rate or vice-versa. FPLUME can also be extended above the NBL, *i.e.* to solve the umbrella region semi-empirically in case of strong plumes. In case of favorable wet aggregation conditions (formation of a liquid water window inside the plume or in presence of ice at the upper regions), the aggregation model predicts an ~~"effective"~~ "effective" grain size distribution considering a single aggregated class. ~~We have tested the model implementation simulating well-studied eruptions (results not shown here) obtaining good agreements.~~ For the aggregation model, two test cases have been considered, the Phase-B of El Chichón 1982 eruption and the 6 May 2010 Eyjafjallajökull eruption phase. For the first case, we got reasonable agreement with the empirical Cornell parameterization using a fractal exponent of $D_{fo} = 2.92$, with wet aggregation occurring under the presence of ice (as expected for large strong plumes). For the second case, we could reproduce the observed total mass fraction of aggregates for plume heights between 6.7 and 8.5 km (a.v.l.). Wet aggregation occurs in this case within a narrow window where conditions for liquid water to form are met. In case of aggregation, results are sensitive to the fractal exponent,

which may range from $D_{fo} = 2.92$ to $D_{fo} = 2.99$. Future studies are necessary to better understand and constrain the role of this parameter.

Code availability

The code FPLUME-1.0 is available under request for research purposes.

Appendix A: Correction factor $\hat{f}$ for mass distribution for top-hat versus Gaussian formalism

Denoting with R the top-hat radius of the plume and with b the Gaussian length scale the relationship between them can be written as (e.g. Davidson, 1986):

$$b^2 = R^2/2 \tag{A1}$$

Assuming a Gaussian profile for the concentration, $C(r)$, the mean value between $r = 0$ (where the concentration is maximum) and $r = R$ is:

$$\langle C \rangle = C_0/R^2 \int_0^\infty r \exp(-r^2/b^2) dr = C_0/(2b^2) \int_0^\infty r \exp(-r^2/b^2) dr = 0.25 C_0 \tag{A2}$$

that implies $\hat{C} = 0.25 C_0$. Following similar calculations we have also:

$$\langle C^2 \rangle = C_0^2/R^2 \int_0^\infty r \exp(-2r^2/b^2) dr = C_0^2/(2b^2) \int_0^\infty r \exp(-2r^2/b^2) dr = 0.125 C_0^2 \tag{A3}$$

$$\langle C^3 \rangle = C_0^3/R^2 \int_0^\infty r \exp(-3r^2/b^2) dr = C_0^3/(2b^2) \int_0^\infty r \exp(-3r^2/b^2) dr = 0.0833 C_0^3 \tag{A4}$$

Therefore if we use average (top-hat) variables in Eq. (34) we need to keep in mind that concentration appears in the nonlinear terms and therefore we should use the following correction factors:

$$\hat{f}_2 = \frac{\langle C^2 \rangle}{\hat{C}^2} = \frac{0.125 C_0^2}{(0.25 C_0)^2} = \frac{0.125 C_0^2}{0.0625 C_0^2} = 2 \tag{A5}$$

$$\hat{f}_3 = \frac{\langle C^3 \rangle}{\hat{C}^3} = \frac{0.0833 C_0^2}{0.015625 C_0^3} = 5.33 \tag{A6}$$

and so on ($\langle \cdot \rangle$ denotes the average using the top-hat filter, e.g. $\hat{C} = \langle C \rangle$). Because terms in Eq.(34) scale with concentration with a power of two we need to account for a correction factor $\hat{f} = \hat{f}_2$. The factor $\hat{f}$ can be also used to correct underestimation of Eulerian time scale with respect Lagrangian time scale (e.g. Dosio et al., 2005).

Appendix B: Computation of n_{tot}

Consider a particle grain size distribution discretized in n bins of width $\Delta\Phi_j$ with the bin center at Φ_j and where Φ_{ja} e Φ_{jb} are the bin limits (*i.e.* $\Delta\Phi_j = \Phi_{jb} - \Phi_{ja}$). The number of particles per unit volume in the bin Φ_j (assuming spherical particles) is:

$$n(\Phi_j) = \int_{\Phi_{ja}}^{\Phi_{jb}} \frac{6C(\Phi)}{\pi\rho(\Phi)d^3(\Phi)}\,\mathrm{d}\Phi \tag{B1}$$

Considering that $d(\Phi) = d_* 2^{-\Phi} = d_* e^{-\Phi\log 2}$ and the top-hat formalism, the above expression can be approached as:

$$n(\Phi_j) \approx \frac{6\hat{C}_j}{\pi\rho_j d_*^3 \Delta\Phi_j} \int_{\Phi_{ja}}^{\Phi_{jb}} e^{3\Phi\log 2}\,\mathrm{d}\Phi = \frac{1}{3\log 2}\left(\frac{6\hat{C}_j}{\pi\rho_j d_*^3\Delta\Phi_j}\right)\left[e^{3\log 2\Phi_{jb}} - e^{3\log 2\Phi_{ja}}\right] \tag{B2}$$

Adding the contribution of all bins, this yields to:

$$n_{tot} = \frac{1}{3\log 2 d_*^3}\sum_j \left(\frac{6\hat{C}_j}{\pi\rho_j\Delta\Phi_j}\right)\left[e^{3\log 2(\Phi_j+\Delta\Phi_j/2)} - e^{3\log 2(\Phi_j-\Delta\Phi_j/2)}\right] \tag{B3}$$

or, in terms of particle diameter:

$$n_{tot} = \frac{1}{3\log 2}\sum_j \left(\frac{6\hat{C}_j}{\pi\Delta\Phi_j\rho_j}\right)\left[\frac{1}{d_{aj}^3} - \frac{1}{d_{bj}^3}\right] \tag{B4}$$

which is Eq. (42).

Acknowledgements. This work was partially supported by the MED-SUV Project funded by the European Union (FP7 Grant Agreement n.308665). We ~~thank~~ acknowledge C. Bonadonna for providing grain size data for the Eyjafjallajökull test case. We thank T. Esposito Ongaro and an anonymous reviewer for their constructive comments.

References

Arason, P., Petersen, G. N., and Bjornsson, H.: Observations of the altitude of the volcanic plume during the eruption of Eyjafjallajökull, April-May 2010, Earth System Science Data, 3, 9–17, doi:10.5194/essd-3-9-2011, http://www.earth-syst-sci-data.net/3/9/2011/, 2011.

Arastoopour, H., Wang, C., and Weil, S.: Particle-particle interaction force in a dilute gas-solid system, Chemical Engineering Science, 37, 1379 – 1386, doi:http://dx.doi.org/10.1016/0009-2509(82)85010-0, http://www.sciencedirect.com/science/article/pii/0009250982850100, 1982.

Bemporad, G. A.: Simulation of round buoyant jets in a stratified flowing environment, J. Hydr. Eng., 120, 529–543, 1994.

Bonadonna, C., Genco, R., Gouhier, M., Pistolesi, M., Cioni, R., Alfano, F., Hoskuldsson, A., and Ripepe, M.: Tephra sedimentation during the 2010 Eyjafjallajökull eruption (Iceland) from deposit, radar, and satellite observations, Journal of Geophysical Research: Solid Earth, 116, n/a–n/a, doi:10.1029/2011JB008462, http://dx.doi.org/10.1029/2011JB008462, b12202, 2011.

Bonasia, R., Costa, A., Folch, A., Macedonio, G., and Capra, L.: Numerical simulation of tephra transport and deposition of the 1982 El Chichón eruption and implications for hazard assessment, Journal of Volcanology and Geothermal Research, 231–232, 39–49, doi:http://dx.doi.org/10.1016/j.jvolgeores.2012.04.006, http://www.sciencedirect.com/science/article/pii/S0377027312000868, 2012.

Brown, R., Bonadonna, C., and Durant, A.: A review of volcanic ash aggregation, Physics and Chemistry of the Earth, 45–46, 65–78, doi:http://dx.doi.org/10.1016/j.pce.2011.11.001, http://www.sciencedirect.com/science/article/pii/S1474706511003172, volcanic ash: an agent in Earth systems, 2012.

Bursik, M.: Effect of wind on the rise height of volcanic plumes, Geophysical Research Letters, 28, 3621–3624, doi:10.1029/2001GL013393, http://doi.wiley.com/10.1029/2001GL013393, 2001.

Carazzo, G., Kaminski, E., and Tait, S.: The route to self-similarity in turbulent jets and plumes, Journal of Fluid Mechanics, 547, 137, doi:10.1017/S002211200500683X, 2006.

Carazzo, G., Kaminski, E., and Tait, S.: On the dynamics of volcanic columns: A comparison of field data with a new model of negatively buoyant jets, Journal of Volcanology and Geothermal Research, 178, 94–103, doi:10.1016/j.jvolgeores.2008.01.002, http://linkinghub.elsevier.com/retrieve/pii/S0377027308000176, 2008a.

Carazzo, G., Kaminski, E., and Tait, S.: On the rise of turbulent plumes: Quantitative effects of variable entrainment for submarine hydrothermal vents, terrestrial and extra terrestrial explosive volcanism, Journal of Geophysical Research, 113, B09 201, doi:10.1029/2007JB005458, http://doi.wiley.com/10.1029/2007JB005458, 2008b.

Carazzo, G., Girault, F., Aubry, T., Bouquerel, H., and Kaminski, E.: Laboratory experiments of forced plumes in a density-stratified crossflow and implications for volcanic plumes, Geophysical Research Letters, 41, 8759–8766, doi:10.1002/2014GL061887, http://dx.doi.org/10.1002/2014GL061887, 2014GL061887, 2014.

Carey, S. N. and Sigurdsson, H.: Influence of particle aggregation on deposition of distal tephra from the MAy 18, 1980, eruption of Mount St. Helens volcano, Journal of Geophysical Research: Solid Earth, 87, 7061–7072, doi:10.1029/JB087iB08p07061, http://dx.doi.org/10.1029/JB087iB08p07061, 1982.

Charpentier, I. and Espíndola, J. M.: A study of the entrainment function in models of Plinian columns: characteristics and calibration, Geophysical Journal International, 160, 1123–1130, doi:10.1111/j.1365-246X.2005.02541.x, http://gji.oxfordjournals.org/cgi/doi/10.1111/j.1365-246X.2005.02541.x, 2005.

Cornell, W., Carey, S., and Sigurdsson, H.: Computer simulation of transport and deposition of the campanian Y-5 ash, Journal of Volcanology and Geothermal Research, 17, 89–109, doi:http://dx.doi.org/10.1016/0377-0273(83)90063-X, http://www.sciencedirect.com/science/article/pii/037702738390063X, explosive Volcanism, 1983.

Costa, A., Macedonio, G., and Folch, A.: A three-dimensional Eulerian model for transport and deposition of volcanic ashes, Earth and Planetary Science Letters, 241, 634–647, 2006.

Costa, A., Folch, A., and Macedonio, G.: A model for wet aggregation of ash particles in volcanic plumes and clouds: 1. Theoretical formulation, Journal of Geophysical Research B: Solid Earth, 115, 2010.

Costa, A., Folch, A., and Macedonio, G.: Density-driven transport in the umbrella region of volcanic clouds: Implications for tephra dispersion models, Geophysical Research Letters, 40, doi:10.1002/grl.50942, http://doi.wiley.com/10.1002/grl.50942, 2013.

Costa, A., Suzuki, Y. J., Cerminara, M., Devenish, B. J., Esposti Ongaro, T., Herzog, M., Van Eaton, A. R., Denby, L. C., Bursik, M., de' Michieli Vitturi, M., Engwell, S., Neri, A., Barsotti, S., Folch, A., Macedonio, G., Girault, F., Carazzo, G., Tait, S., Kaminski, E., Mastin, L. G., Woodhouse, M. J., Phillips, J. C., Hogg, A. J., Degruyter, W., and Bonadonna, C.: Results of the eruption column model inter-comparison exercise, J. Volcanol. Geotherm. Res., accepted, 2015.

Craske, J., Debugne, A., and van Reeuwijk, M.: Shear-flow dispersion in turbulent jets, Journal of Fluid Mechanics, 781, 28–51, doi:10.1017/jfm.2015.417, http://journals.cambridge.org/article_S0022112015004176, 2015.

Davidson, G. A.: Gaussian versus top-hat profile assumptions in integral plume models, Atmospheric Environment, 20, 417–478, 1986.

de' Michieli Vitturi, M., Neri, A., and Barsotti, S.: PLUME-MoM 1.0: a new 1-D model of volcanic plumes based on the method of moments, Geoscientific Model Development Discussions, 8, 3745–3790, doi:10.5194/gmdd-8-3745-2015, http://www.geosci-model-dev-discuss.net/8/3745/2015/, 2015.

Degruyter, W. and Bonadonna, C.: Improving on mass flow rate estimates of volcanic eruptions, Geophysical Research Letters, 39, n/a–n/a, doi:10.1029/2012GL052566, http://dx.doi.org/10.1029/2012GL052566, l16308, 2012.

Dellino, P., Mele, D., Bonasia, R., Braia, G., La Volpe, L., and Sulpizio, R.: The analysis of the influence of pumice shape on its terminal velocity, Geophysical Research Letters, 32, n/a–n/a, doi:10.1029/2005GL023954, http://dx.doi.org/10.1029/2005GL023954, 2005.

Dellino, P., Dioguardi, F., Mele, D., D'Addabbo, M., Zimanowski, B., Büttner, R., Doronzo, D. M., Sonder, I., Sulpizio, R., Dürig, T., and La Volpe, L.: Volcanic jets, plumes, and collapsing fountains: Evidence from large-scale experiments, with particular emphasis on the entrainment rate, Bulletin of Volcanology, 76, 1–18, doi:10.1007/s00445-014-0834-6, 2014.

Devenish, B.: Using simple plume models to refine the source mass flux of volcanic eruptions according to atmospheric conditions, Journal of Volcanology and Geothermal Research, 256, 118 –

127, doi:http://dx.doi.org/10.1016/j.jvolgeores.2013.02.015, http://www.sciencedirect.com/science/article/pii/S0377027313000668, 2013.

Dosio, A., Vila-Guerau de Arelano, J., and Holstlag, A.: Relating Eulerian and Lagrangian Statistics for the Turbulent Dispersion in the Atmospheric Convective Boundary Layer, Journal of the Atmospheric Sciences, 62, 1175 – 1191, 2005.

Durant, A. J., Rose, W. I., Sarna-Wojcicki, A. M., Carey, S., and Volentik, A.: Hydrometeor-enhanced tephra sedimentation: Constraints from the 18 May 1980 eruption of Mount St. Helens, Journal of Geophysical Research: Solid Earth, 114, n/a–n/a, doi:10.1029/2008JB005756, http://dx.doi.org/10.1029/2008JB005756, b03204, 2009.

Ernst, G., Sparks, R. S. J., Carey, S., and Bursik, M.: Sedimentation from turbulent jets and plumes, Journal of Geophysical Research, 101, 5575–5589, http://onlinelibrary.wiley.com/doi/10.1029/95JB01900/full, 1996.

Esposti Ongaro, T., Cavazzoni, C., Erbacci, G., Neri, A., and Salvetti, M.: A parallel multiphase flow code for the 3D simulation of explosive volcanic eruptions, Parallel Computing, 33, 541 – 560, doi:http://dx.doi.org/10.1016/j.parco.2007.04.003, http://www.sciencedirect.com/science/article/pii/S0167819107000634, 2007.

Folch, A.: A review of tephra transport and dispersal models: Evolution, current status, and future perspectives, Journal of Volcanology and Geothermal Research, 235-236, 96–115, 2012.

Folch, A., Costa, A., and Macedonio, G.: FALL3D: A computational model for transport and deposition of volcanic ash, Computers and Geosciences, 35, 1334 – 1342, doi:http://dx.doi.org/10.1016/j.cageo.2008.08.008, http://www.sciencedirect.com/science/article/pii/S0098300408002781, 2009.

Folch, A., Costa, A., Durant, A., and Macedonio, G.: A model for wet aggregation of ash particles in volcanic plumes and clouds: 2. Model application, Journal of Geophysical Research, 115, B09 202, doi:10.1029/2009JB007176, http://doi.wiley.com/10.1029/2009JB007176, 2010.

Frenklach, M.: Method of moments with interpolative closure, Chem. Eng. Sci., 57, 2229–2239, 2002.

Ganser, G. H.: A rational approach to drag prediction of spherical and nonspherical particles, Powder Technology, 77, 143 – 152, doi:http://dx.doi.org/10.1016/0032-5910(93)80051-B, http://www.sciencedirect.com/science/article/pii/003259109380051B, 1993.

Gmachowski, L.: Calculation of the fractal dimension of aggregates, Colloids and Surfaces A: Physicochemical and Engineering Aspects, 211, 197–203, doi:http://dx.doi.org/10.1016/S0927-7757(02)00278-9, http://www.sciencedirect.com/science/article/pii/S0927775702002789, 2002.

Gudmundsson, M., Thordarson, T., Höskuldsson, A., Larsen, G., Björnsson, H., Prata, F., Oddsson, B., Magnüsson, E., Högnadoóttir, T., Petersen, G., Hayward, C., Stevenson, J., and Jónsdóttir: Ash generation and distribution from the April-May 2010 eruption of Eyjafjallajökull, Iceland, Nature Scientific Reports, pp. 1–12, doi:10.1038/srep00572, 2012.

Herzog, M. and Graf, H.-F.: Applying the three-dimensional model ATHAM to volcanic plumes: Dynamic of large co-ignimbrite eruptions and associated injection heights for volcanic gases, Geophysical Research Letters, 37, n/a–n/a, doi:10.1029/2010GL044986, http://dx.doi.org/10.1029/2010GL044986, l19807, 2010.

Hewett, T. A., Fay, J. A., and Hoult, D. P.: Laboratory experiments of smokestack plumes in a stable atmosphere, Atmospheric Environment (1967), 5, 767–789, doi:10.1016/0004-6981(71)90028-X, http://linkinghub.elsevier.com/retrieve/pii/000469817190028X, 1971.

Hindmarsh, A.: Lsode and lsodi, two new initial value ordinary differential equations solvers, Acm-Signum Newsl., 4, 10–11, 1980.

Jacobson, M. Z.: Fundamentals of atmospheric modelling, Cambridge University Press, New York, 2nd edn. edn., 2005.

Jullien, R. and Botet, R.: Aggregation and fractal aggregates, World Sci., Singapore, 1987.

Kaminski, E., Tait, S., and Carazzo, G.: Turbulent entrainment in jets with arbitrary buoyancy, Journal of Fluid Mechanics, 526, 361–376, doi:10.1017/S0022112004003209, http://www.journals.cambridge.org/abstract_S0022112004003209, 2005.

Krumbein, W. C.: Size frequency distributions of sediments, J. Sediment. Res., 4, 65–67, 1934.

Lee, J. H. and Cheung, V.: Generalized Lagrangian Model for Buoyant Jets in Current, J. Env. Eng., 116, 1085–1106, 1990.

Mastin, L., Guffanti, M., Servranckx, R., Webley, P., Barsotti, S., Dean, K., Durant, A., Ewert, J., Neri, A., Rose, W., Schneider, D., Siebert, L., Stunder, B., Swanson, G., Tupper, A., Volentik, A., and Waythomas, C.: A multidisciplinary effort to assign realistic source parameters to models of volcanic ash-cloud transport and dispersion during eruptions, Journal of Volcanology and Geothermal Research, 186, 10 – 21, doi:http://dx.doi.org/10.1016/j.jvolgeores.2009.01.008, http://www.sciencedirect.com/science/article/pii/S0377027309000146, improved Prediction and Tracking of Volcanic Ash Clouds, 2009.

Morton, B. R., Taylor, G. I., and Turner, J. S.: Turbulent gravitational convection from maintained and instantaneous source, Proceedings of the Royal Society of London, 234, 1–23, 1956.

Murphy, D. M. and Koop, T.: Review of the vapour pressures of ice and supercooled water for atmospheric applications, Quarterly Journal of the Royal Meteorological Society, 131, 1539–1565, doi:10.1256/qj.04.94, http://dx.doi.org/10.1256/qj.04.94, 2005.

Netterville, D. D. J.: Plume rise, entrainment and dispersion in turbulent winds, Atmospheric Environment. Part A. General Topics, http://www.sciencedirect.com/science/article/pii/096016869090074W, 1990.

Pruppacher, H. R. and Klett, J. D.: Microphysics of Clouds and Precipitation, Springer, 1st edn., 1996.

Rose, W. and Durant, A.: El Chichón volcano, April 4, 1982: volcanic cloud history and fine ash fallout, Natural Hazards, 51, 363–374, doi:10.1007/s11069-008-9283-x, http://dx.doi.org/10.1007/s11069-008-9283-x, 2009.

Rouse, H., Yih, C. S., and Humphreys, H. W.: Gravitational convection from a boundary source, Tellus, 4, 201–210, 1952.

Schneider, D. J., Rose, W. I., Coke, L. R., and Bluth, G. J. S.: Early evolution of a stratospheric volcanic eruption cloudas observed with TOMS and AVI-IRR, Journal of Geophysical Research, 104, 4037–4050, 1999.

Sigurdsson, H., Carey, S., and Espindola, J.: The 1982 eruptions of El Chichón Volcano, Mexico: Stratigraphy of pyroclastic deposits, Journal of Volcanology and Geothermal Research, 23, 11–37, doi:http://dx.doi.org/10.1016/0377-0273(84)90055-6, http://www.sciencedirect.com/science/article/pii/0377027384900556, 1984.

Sparks, R.: The dimensions and dynamics of volcanic eruption columns, Bulletin of Volcanology, 48, 3–15, doi:10.1007/BF01073509, http://dx.doi.org/10.1007/BF01073509, 1986.

Sparks, R. S. J.: Volcanic plumes, Chichester ; New York : Wiley, c1997, 1997.

Suzuki, Y. J. and Koyaguchi, T.: A three-dimensional numerical simulation of spreading umbrella clouds, Journal of Geophysical Research, 114, B03 209, doi:10.1029/2007JB005369, http://doi.wiley.com/10.1029/2007JB005369, 2009.

Suzuki, Y. J. and Koyaguchi, T.: 3D numerical simulation of volcanic eruption clouds during the 2011 Shinmoedake eruptions, Earth, Planets and Space, 65, 581–589, doi:10.5047/eps.2013.03.009, 2013.

Suzuki, Y. J. and Koyaguchi, T.: Effects of wind on entrainment efficiency in volcanic plumes, J. Geophys. Res., accepted, 2015.

Suzuki, Y. J., Koyaguchi, T., Ogawa, M., and Hachisu, I.: A numerical study of turbulent behaviour in eruption clouds using a three dimensional fluid dynamics model, Journal of Geophysical Research, 110, B08 201, doi:10.1029/2004JB003460, 2005.

Tate, P. M.: The rise and dilution of buoyant jets and their behaviour in an internal wave field, PhD. thesis, University of New South Wales, http://www.library.unsw.edu.au/~thesis/adt-NUN/public/adt-NUN20040527.120914/index.html, 2002.

Wang, H. and Wing-Keung Law, A.: Second-order integral model for a round turbulent buoyant jet, Journal of Fluid Mechanics, 459, 397–428, doi:10.1017/S0022112002008157, http://journals.cambridge.org/article_S0022112002008157, 2002.

Wilson, L.: Explosive Volcanic Eruptions, III. Plinian Eruption Columns, Geophysical Journal International, 45, 543–556, doi:10.1111/j.1365-246X.1976.tb06909.x, http://gji.oxfordjournals.org/content/45/3/543.abstract, 1976.

Wilson, L. and Huang, T. C.: The influence of shape on the atmospheric settling velocity of volcanic ash particles, Earth and Planetary Science Letters, 44, 311 – 324, doi:http://dx.doi.org/10.1016/0012-821X(79)90179-1, http://www.sciencedirect.com/science/article/pii/0012821X79901791, 1979.

Woodhouse, M. J., Hogg, A. J., Phillips, J. C., and Sparks, R. S. J.: Interaction between volcanic plumes and wind during the 2010 Eyjafjallajökull eruption, Iceland, Journal of Geophysical Research: Solid Earth, 118, 92–109, doi:10.1029/2012JB009592, 2013.

Woods, A. W.: Moist convection and the injection of volcanic ash into the atmosphere, Journal of Geophysical Research, 98, 17 627, doi:10.1029/93JB00718, 1993.

Woods, A. W. and Kienle, J.: The dynamics and thermodynamics of volcanic clouds: Theory and observations from the April 15 and April 21, 1990 eruptions of Redoubt Volcano, Alaska, J. Volcanol. Geotherm. Res., 62, 273–299, 1994.

Xiong, C. and Friedlander, S. K.: Morphological properties of atmospheric aerosol aggregates, Proc. Nat. Acad. Sci. USA, 98, 11,851–11,856, doi:10.1073/pnas.211376098, 2001.

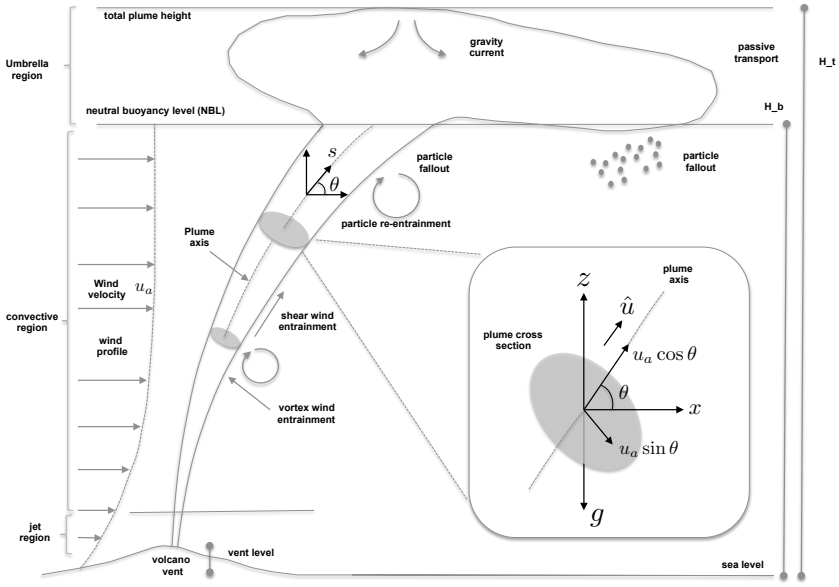

Figure 1. Sketch of an axisymmetric volcanic plume raising in a wind profile. Three different regions (jet thrust, convective thrust and umbrella) are indicated, with the convective region reaching a height H_b (that of the neutral buoyancy level), and the umbrella region raising up to H_t above the sea level (a.s.l.). The inset plot details a plume cross-section perpendicular to the plume axis, inclined of an angle θ with respect to the horizontal.

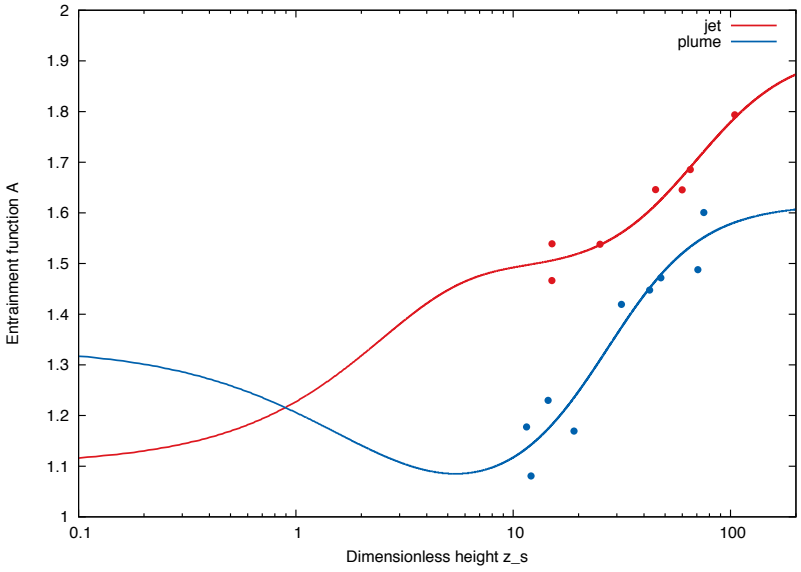

Figure 2. Entrainment functions $A(z_s)$ for jets and plumes depending on the dimensionless height $z_s = z/2r_o$. Functions have been obtained by fitting experimental data (points) from Carazzo et al. (2006) (for $z_s > 10$) and multiplying by a correction function (20c) to extend the functions to $z_s < 10$ verifying function continuity and convergence to values of $A = 1.11$ for jets and $A = 1.31$ for plumes when $z_s \to 0$.

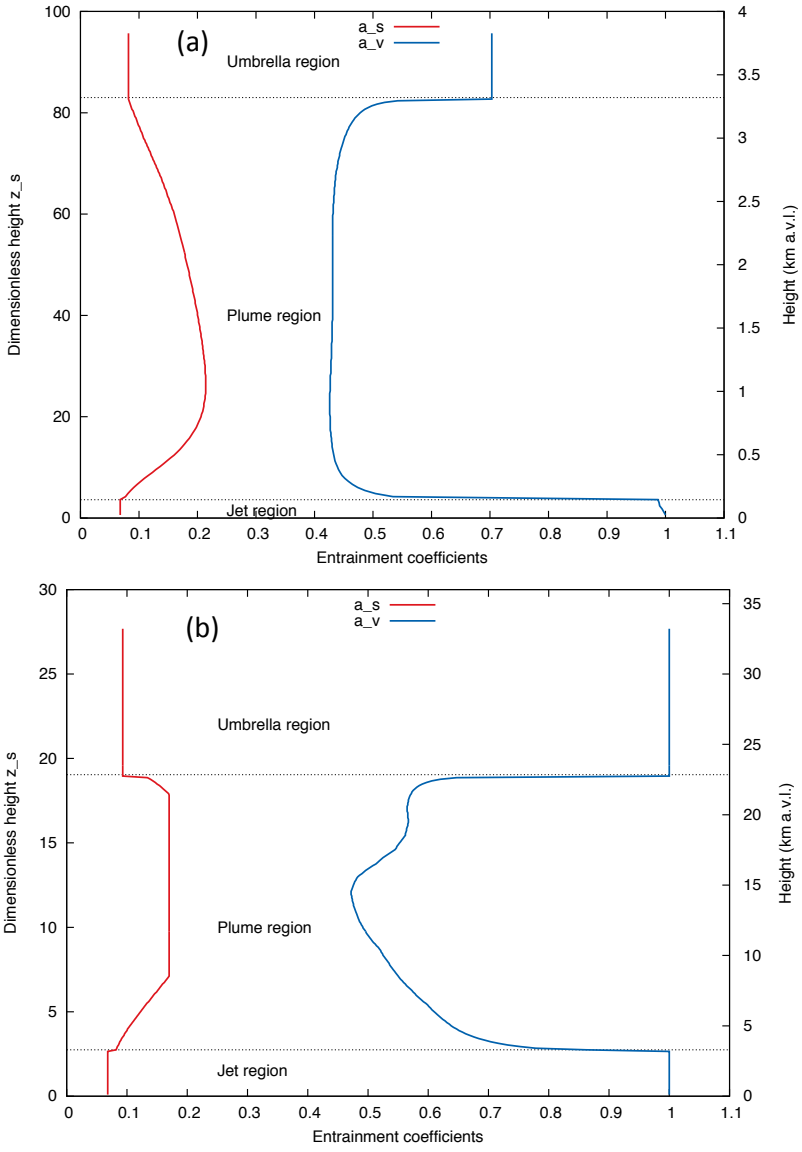

Figure 3. Entrainment coefficients α_s (red) and α_v (blue) versus height for weak (a) and strong (b) plumes under a wind profile. The vertical dashed lines indicate the transition between the different eruptive column regions. Weak plume simulation with: $\hat{M}_o = 1.5 \times 10^6$ kgs^{-1}, $\hat{u}_o = 135$ ms^{-1}, $\hat{T}_o = 1273$ K, $\hat{x}_{wo} = 0.03$. Strong plume simulation with: $\hat{M}_o = 1.5 \times 10^9$ kgs^{-1}, $\hat{u}_o = 300$ ms^{-1}, $\hat{T}_o = 1153$ K, $\hat{x}_{wo} = 0.05$.

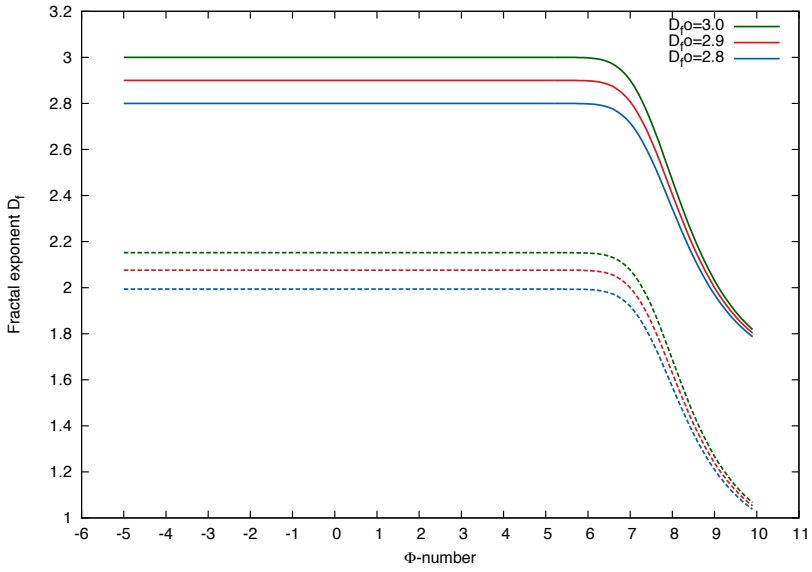

Figure 4. Dependency of fractal exponent D_f (continuous lines) and fractal pre-factor k_f (dashed lines) on particle size expressed in Φ units according to equations (32) and (33) for different values of D_{fo}. Note the progressive decay in D_f starting at $\Phi = 7$ ($d \approx 10\mu\mathrm{m}$) and leading to values of $D_f = 1.6$ for $\Phi = 9$ ($d \approx 2\mu\mathrm{m}$).

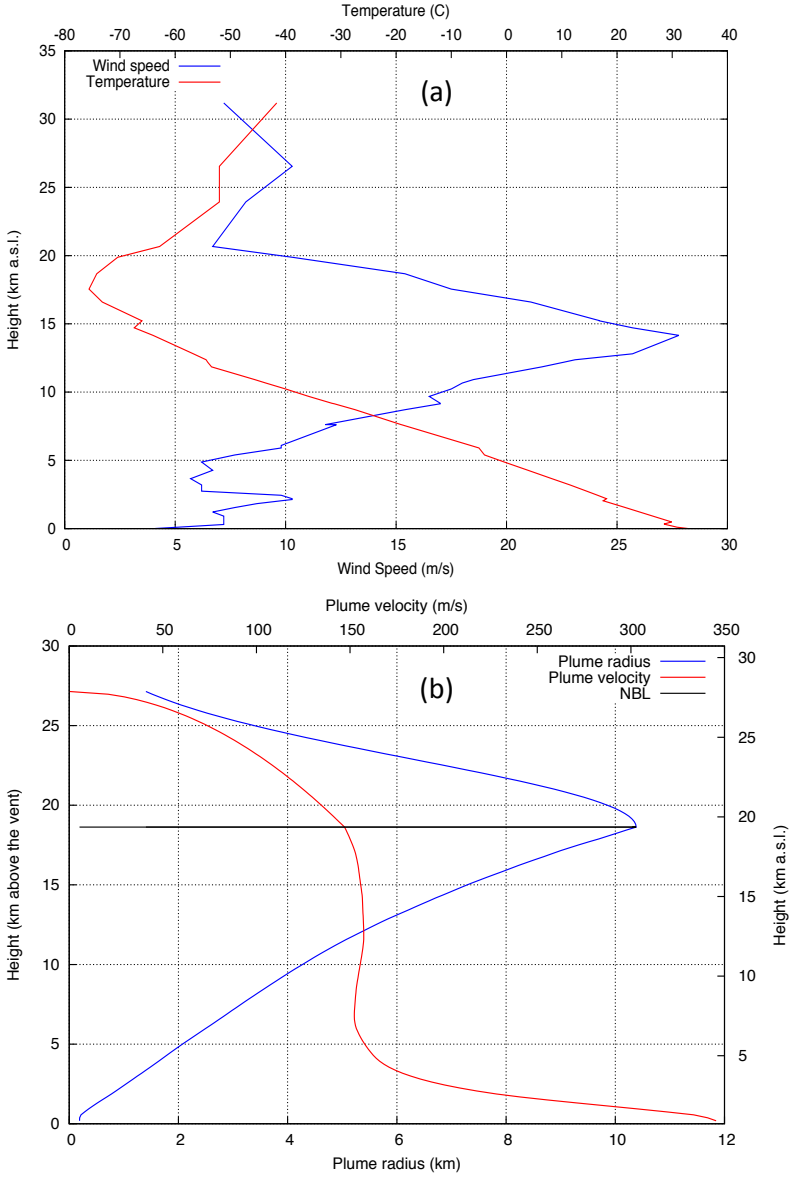

Figure 5. (a): wind and temperature atmospheric profiles during 4 April 1982 at 00UTC from sounding. (b): FPLUME bulk velocity $\hat{u}$ and radius r with height z. The black solid line indicates the height of the NBL determined by the model.

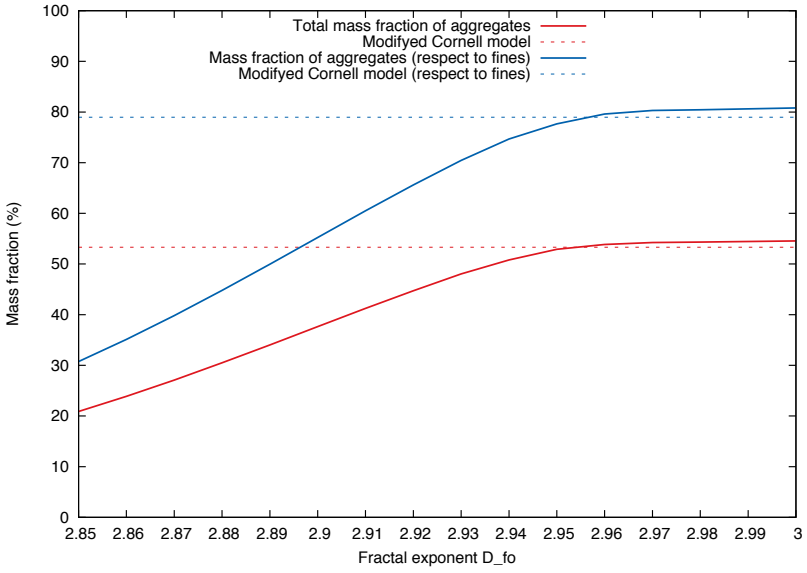

Figure 6. El Chichón 1982 phase-B simulation. Total mass fraction of aggregates (red line) and total mass fraction of aggregates with respect to fines (blue line) depending on the fractal exponent D_{fo}. The (constant) values predicted by the modified Cornell model are shown by dashed lines.

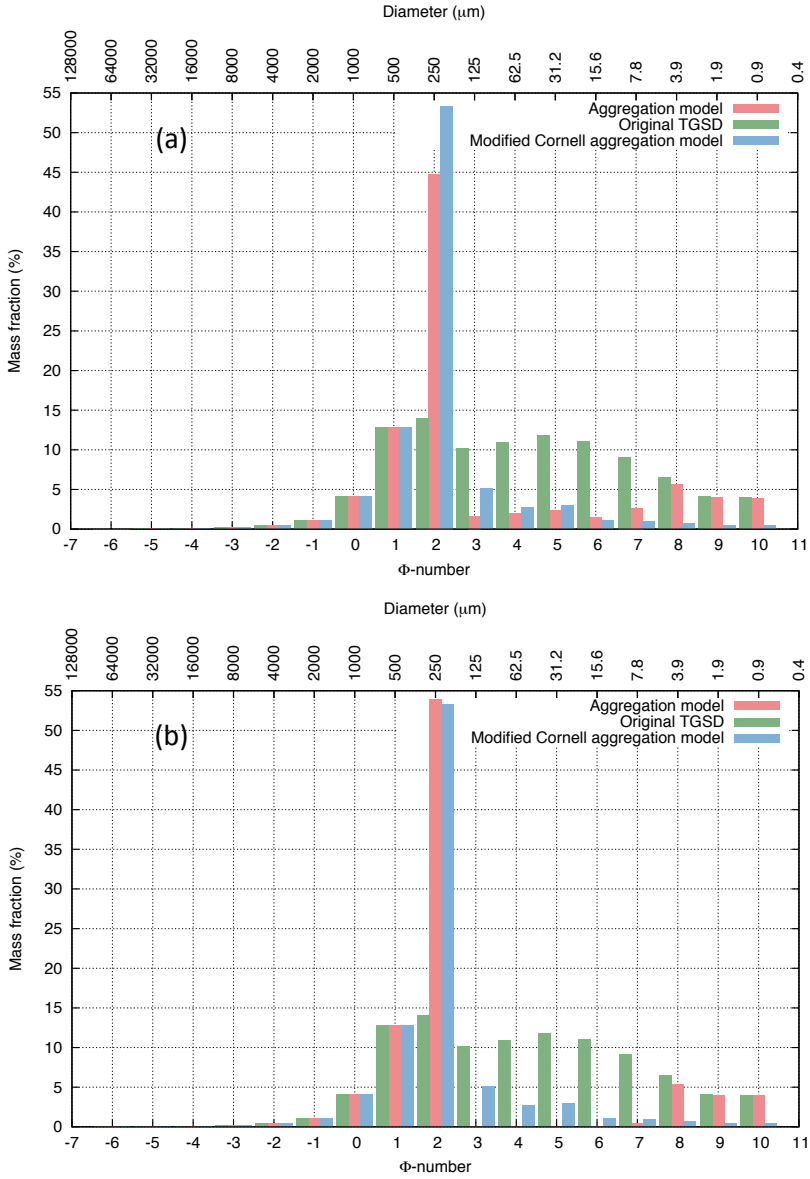

Figure 7. Results of the aggregation model in FPLUME for El Chichón 1982 phase-B simulation. Green bars show the original TGSD from Rose and Durant (2009) discretized in 17 Φ-classes. Blue bars show the results of the modified Cornell model. Finally, read bars give the results of our wet aggregation model considering a fractal exponent of ~~$D_{fo} = 2.96$~~ $D_{fe} = 2.92$ (a) and ~~$D_{fo} = 2.92$~~ $D_{fe} = 2.96$ (b).

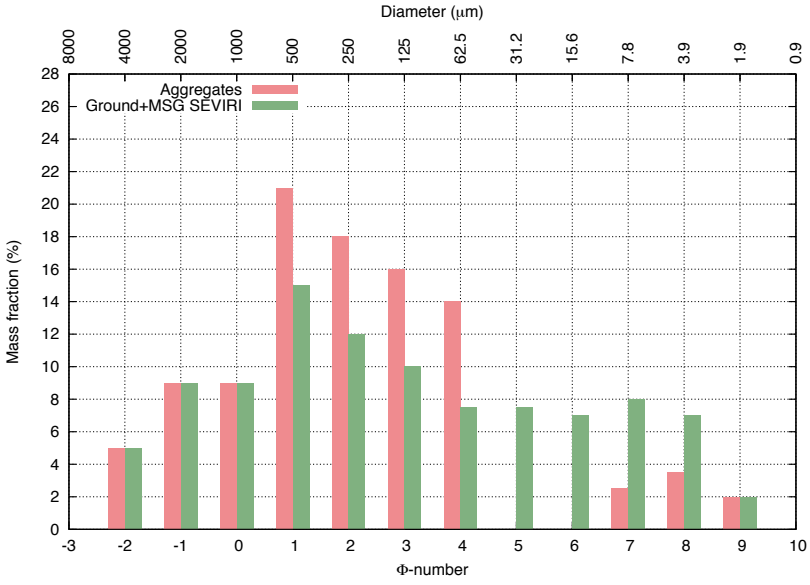

Figure 8. Original grain size distribution from ground data and MSG-SEVIRI retrievals (green) and distribution modified by aggregation (red). Results are for 6 May 30 minutes averaged. Figure reproduced from Bonadonna et al. (2011) (Figure 17d).

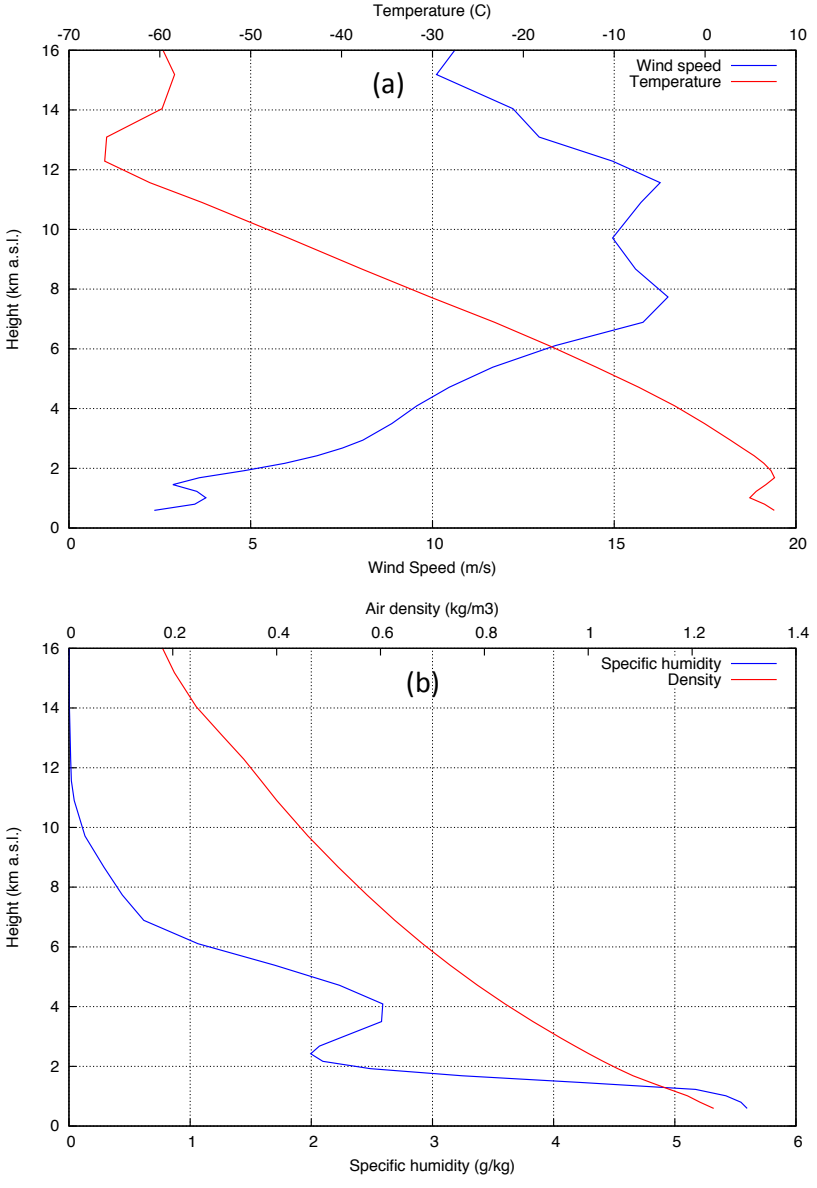

Figure 9. Atmospheric profiles extracted form ERA-Interim re-analysis dataset at Eyjafjallajökull vent location for 6 May 2010 at 12 UTC. (a): wind and temperature profiles. (b): specific humidity and air density profiles.

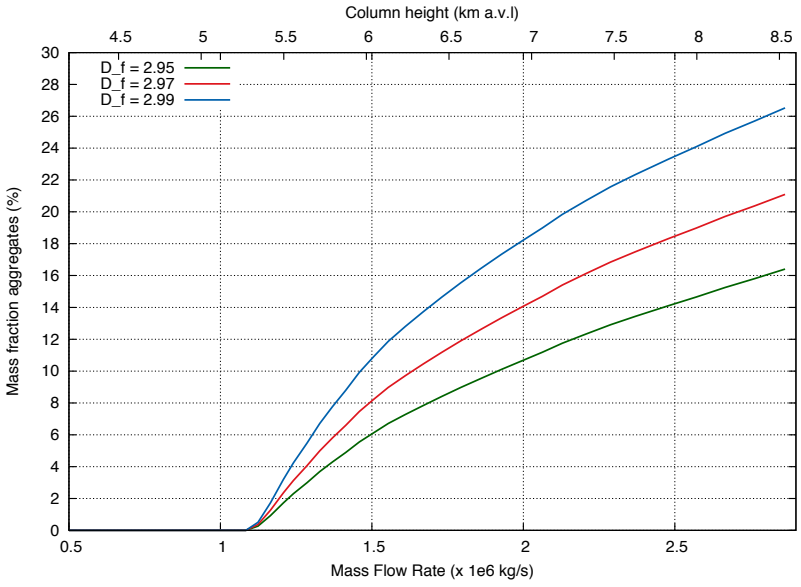

Figure 10. FPLUME aggregation model results for Eyjafjallajökull 6 May phase. Total mass fraction of aggregates (in %) versus mass flow rate (in $\mathrm{kg/s}$) and column height (in km a.v.l.) for different values of the fractal exponent D_{fo} (in these simulations we used $c_H = 1.1$ and the presence of meteoritic water in the plume was not considered). The model predicts a 10% in mass of wet aggregates for column heights between ~~6.7~~ 6.0 and ~~7.5~~ 7.0 km (a.v.l.). Input parameters were fixed as in Table 5 varying mass flow rate (column height).

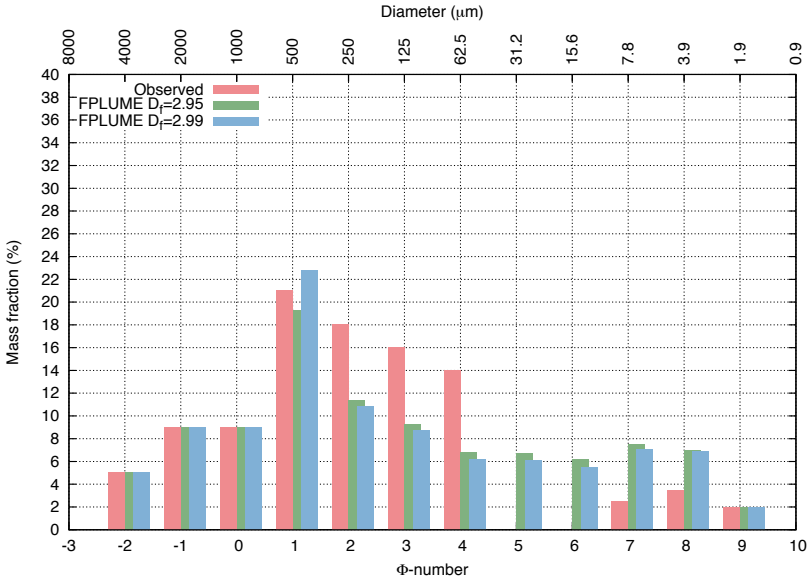

Figure 11. Grain size distribution predicted by the wet aggregation model for Eyjafjallajökull 6 May phase for a column height of ~~7~~ 6.5 km (a.v.l.) for two different values of the fractal exponent D_{fo} of 2.95 and 2.99. Observed data from Bonadonna et al. (2011).

Table 1. List of latin symbols. Quantities with a hat denote bulk (top-hat averaged) quantities. Throughout the text, the subindex o (*e.g.* $\hat{M}_o$, $\hat{u}_o$, etc.) indicates values of quantities at the vent ($s = 0$).

Symbol	Definition	Units
$A_i^+(A_i^-)$	Aggregation source (sink) terms	kgs^{-1}
A_B	Collision frequency by Brownian motion	$\mathrm{m}^3\mathrm{s}^{-1}$
A_{DS}	Collision frequency by differential sedimentation	$\mathrm{m}^{-1}\mathrm{s}$
A_S	Collision frequency by fluid shear	s^{-1}
A_{TI}	Collision frequency by turbulent inertia	$\mathrm{m}^3\mathrm{s}^{-1}$
~~$\hat{c}$ Specific heat capacity of the mixture Given by eq. (??)~~ c_a	Specific heat capacity of air at constant pressure	Jkg^{-1}
c_l	Specific heat capacity of liquid water	Jkg^{-1}
c_p	Specific heat capacity of particles (pyroclasts)	Jkg^{-1}
c_s	Specific heat capacity of solid water (ice)	Jkg^{-1}
c_v	Specific heat capacity of water ~~vapor~~ vapour	Jkg^{-1}
C_d	Particle drag coefficient	-
$\hat{C}_i$	Mass concentration of particles of class i	kgm^{-}
D_f	Fractal exponent	-
d_A	Diameter of the aggregates	m
d_i	Diameter of particles of class i	m
e_l	Saturation pressure of water ~~vapor~~ vapour over liquid	Pa
e_s	Saturation pressure of water ~~vapor~~ vapour over solid (ice)	Pa
$\hat{E}$	Energy flow rate	kgm^2
$\hat{f}$	Correction factor for aggregation	-
f	Particle re-entrainment parameter	-
f_i	Mass fraction of particle class i	-
g	Gravitational acceleration	ms^{-2}
~~k_b~~ h_l	~~Boltzmann constant~~ Enthalpy per unit mass of liquid water	$\mathrm{J\,kg}^{-1}$
~~L_c~~ h_s	~~Latent heat of water vapor condensation~~ Enthalpy per unit mass of ice	$\mathrm{J\,kg}^{-1}$
~~L_d~~ h_v	~~Latent heat of water vapor deposition~~ Enthalpy per unit mass of vapour	$\mathrm{J\,kg}^{-1}$
h_{l0}	Enthalpy per unit mass of liquid water at $T = T_0$	$\mathrm{J\,kg}^{-1}$
h_{s0}	Enthalpy per unit mass of ice at $T = T_0$	$\mathrm{J\,kg}^{-1}$
h_{v0}	Enthalpy per unit mass of vapour at $T = T_0$	$\mathrm{J\,kg}^{-1}$
h_{wa}	Enthalpy per unit mass of water in the atmosphere	$\mathrm{J\,kg}^{-1}$
$\hat{M}$	Total mass flow rate	kgs^{-1}
$\hat{M}_a$	Mass flow rate of dry air	kgs^{-1}
$\hat{M}_i$	Mass flow rate of particles of class i	kgs^{-1}
$\hat{M}_w$	Mass flow rate of volatiles (water in any phase)	kgs^{-1}
N_i	Number of particles of diameter d_i in an aggregate	-
$\dot{n}_i$	Number of aggregating particles per unit volume and time	$\mathrm{m}^{-3}\mathrm{s}$
$\dot{n}_{tot}$	Total particle decay per unit volume and time	$\mathrm{m}^{-3}\mathrm{s}$
n_{tot}	Number of particles per unit volume available for aggregation	m^{-3}
$\hat{P}$	Axial (stream-wise) momentum flow rate	kgms
P	Pressure	Pa
P_v	Partial pressure of water ~~vapor~~ vapour	Pa
r	Cross-section plume radius	m
s	Distance along the plume axis	m

Table 2. List of greek symbols. Quantities with a hat denote bulk (top-hat averaged) quantities.

Symbol	Definition	Units	Comments
α_m	Class-averaged particle sticking efficiency	-	Given by ~~eq~~Eq. (44)
α_{ij}	Sticking efficiency between particles of class i and j	-	Given by ~~eq~~Eq.
α_s	stream-wise (shear) air entrainment coefficient	-	Given by ~~eq~~Eq. (19)
α_v	cross-flow (vortex) air entrainment coefficient	-	Given by ~~eq~~Eq. (21)
ϵ	Dissipation rate of turbulent kinetic energy	$\mathrm{m^2s^{-3}}$	Given by ~~eq~~Eq. (37)
Γ_s	Fluid shear	$\mathrm{s^{-1}}$	Given by ~~eq~~Eq. (39)
ϕ	Volume fraction of particles	-	
$\hat{\mu}$	Mixture dynamic viscosity	$\mathrm{Pa\,s}$	Assumed equal to that of air at bulk temperature
μ_l	Liquid water dynamic viscosity	$\mathrm{Pa\,s}$	
$\hat{\nu}$	Mixture kinematic viscosity	$\mathrm{m^2s^{-1}}$	$\hat{\nu} = \hat{\mu}/\hat{\rho}$
$\hat{\rho}$	Mixture density	$\mathrm{kgm^{-3}}$	Given by ~~eq~~Eq. (3)
ρ_a	Ambient air density	$\mathrm{kgm^{-3}}$	Assumed to vary only with z
ρ_l	Liquid water density	$\mathrm{kgm^{-3}}$	Value of 1000
ρ_g	Gas phase (dry air plus water ~~vapor~~vapour) density	$\mathrm{kgm^{-3}}$	
ρ_p	Class-averaged particle (pyroclasts) density	$\mathrm{kgm^{-3}}$	$\rho_p = \sum f_i \rho_{pi}$
ρ_{pi}	Density of particles of class i	$\mathrm{kgm^{-3}}$	
ρ_s	Ice density	$\mathrm{kgm^{-3}}$	Value of 920
ϕ	Solid (particles) volume fraction	-	$\phi = \sum \hat{C}_i/\rho_{pi}$
Φ	Dimensionless number related to size	-	Given by ~~eq~~Eq.(1)
Φ_a	Horizontal wind direction (azimuth)	rad	
Ψ	Particle sphericity	-	$\Psi = 1$ for spheres
θ	Plume bent over angle with respect to the horizontal	rad	
ξ	Diameter to volume fractal relationship	-	
χ	Constant giving the probability of fallout	-	Value of ≈ 0.23 (Bursik, 2001)

Table 3. Constants defining the entrainment functions for jets and plumes following the formulation introduced by Kaminski et al. (2005) (see ~~eq~~Eq. 20a to 20c) obtained after fitting experimental data reported in Carazzo et al. (2006). For Kaminski-R we considered all data including that of Rouse et al. (1952), whereas for Kaminski-C, as suggested by Carazzo et al. (2006), data from Rouse et al. (1952) was excluded.

	Kaminski-R		Kaminski-C	
	jets	plumes	jets	plumes
c_0	1.92	1.61717	1.92	1.55
c_1	3737.26	478.374	3737.26	329.0
c_2	4825.98	738.348	4825.98	504.5
$c_3 = 2(c_2 - c_1)$	2177.44	519.948	1883.81	351.0
c_4	0.00235	-0.00145	0.00235	-0.00145

Table 4. Input values for the El Chichón Phase-B simulation. Values for specific heats of water vapour, liquid water, ice, pyroclasts and air at constant pressure are assigned to defaults of 1900, 4200, 2000, 1600, and 1000 $\mathrm{Jkg^{-1}K^{-1}}$

Parameter	Symbol	Units	Value
Phase start		h	1:35 UTC
Phase end		h	6:00 UTC
Exit velocity	$\hat{u}_o$	$\mathrm{ms^{-1}}$	350
Exit temperature	$\hat{T}_o$	K	1123
~~Magmatic~~ Water mass fraction	$\hat{w}_o$	–	4%
Diameter aggregates	d_A	µm	250
Density aggregates	$\hat{\rho}_A$	$\mathrm{kgm^{-3}}$	200
Probability of particle fallout	χ	–	0.23
Shear entrainment coefficient	α_s	–	~~eq~~Eq.(19)
Vortex entrainment coefficient	α_v	–	~~eq~~Eq.(21)

Table 5. FPLUME input values for the 6 May Eyjafjallajökull simulation. Values for specific heats of water vapour, liquid water, ice, pyroclasts and air at constant pressure are assigned to defaults of 1900, 4200, 2000, 1600, and 1000 $\mathrm{Jkg^{-1}K^{-1}}$

Parameter	Symbol	Units	Value
Phase start		h	06:00 UTC
Phase end		h	12:00 UTC
Exit velocity	$\hat{u}_o$	$\mathrm{ms^{-1}}$	150
Exit temperature	$\hat{T}_o$	K	1200
~~Magmatic~~ Water mass fraction	$\hat{w}_o$	–	3%
Diameter aggregates	d_A	µm	500
Density aggregates	$\hat{\rho}_A$	$\mathrm{kgm^{-3}}$	200
Probability of particle fallout	χ	–	0.23
Shear entrainment coefficient	α_s	–	~~eq~~Eq.(19)
Vortex entrainment coefficient	α_v	–	~~eq~~Eq.(21)